

# **Deep Transformational Calibration of Soft Embedded Sensors for Soft Surgical Robots**

**Navid Masoumi**

**A Thesis**

**in**

**The Department**

**of**

**Mechanical, Industrial, and Aerospace Engineering**

**Presented in Partial Fulfillment of the Requirements**

**for the Degree of**

**Master of Applied Science (Mechanical Engineering) at**

**Concordia University**

**Montréal, Québec, Canada**

**January 2025**

**© Navid Masoumi, 2025**

CONCORDIA UNIVERSITY

School of Graduate Studies

This is to certify that the thesis prepared

By: **Navid Masoumi**

Entitled: **Deep Transformational Calibration of Soft Embedded Sensors for Soft Surgical Robots**

and submitted in partial fulfillment of the requirements for the degree of

**Master of Applied Science (Mechanical Engineering)**

complies with the regulations of this University and meets the accepted standards with respect to originality and quality.

Signed by the Final Examining Committee:

\_\_\_\_\_  
*Dr. Hamid Taghavifar* Chair

\_\_\_\_\_  
*Dr. Christopher Yee Wong* External Examiner

\_\_\_\_\_  
*Dr. Hamid Taghavifar* Examiner

\_\_\_\_\_  
*Dr. Javad Dargahi* Supervisor

\_\_\_\_\_  
*Dr. Amir Hooshir* Co-supervisor

Approved by \_\_\_\_\_  
Muthukumaran Packirisamy, Chair  
Department of Mechanical, Industrial, and Aerospace Engineering

\_\_\_\_\_ 2025

\_\_\_\_\_  
Mourad Debbabi, Dean  
Faculty of Engineering and Computer Science

# Abstract

## Deep Transformational Calibration of Soft Embedded Sensors for Soft Surgical Robots

Navid Masoumi

In this thesis, a novel soft sensor calibration method is proposed for minimally invasive surgery (MIS), based on a gelatin-graphite sensor with high compliance and adaptability developed in previous studies. This approach uses convolutional deep learning that accounts for a sensor's non-linear behavior and reduces noise amplification. This technique offers a smaller minimum detectable force than other approaches and is particularly useful in sensitive surgical scenarios. The sensor's performance is characterized by its fine resolution ( $\leq 1\text{mN}$ ) and accurate force estimation, especially for forces below 400 mN of amplitude. The best calibration (Morse) scheme provides high performance, with a Mean Absolute Error of  $\leq 7.9$  mN. This work was validated through comparison among other representative studies and offered a path toward future directions for optimizing and implementing soft robotic sensors in minimally invasive surgeries. The application of this sensor can revolutionize surgical procedures and capitalize on the benefits of soft robotics, potentially enhancing precision and reducing trauma in surgeries. Building on the established capabilities of this calibration method, the thesis further explores its integration with the surgical applications. This integration aims to provide surgeons with a tactile sense that mimics natural touch, thereby improving the control and safety of surgeries. Future studies will aim to enhance the sensor's performance in minimally invasive surgeries by extending the force sensing range through optimization of material properties and structural design, implementing precise micro-fabrication techniques, developing advanced real-time calibration methods, and integrating the sensor into surgical robotics to evaluate its performance in controlled, simulated MIS scenarios where sensor's accuracy is validated using physical phantoms to mimic endoluminal procedures.

# Acknowledgments

This thesis marks the peak of a challenging yet rewarding two-year master's program. Over the past two years, I have been on a truly unique journey filled with its own set of challenges. This was a rich blend of learning, facing difficult days, and reveling in joyful moments, making it a distinctive chapter in my life. These experiences have profoundly shaped my future in ways I had never anticipated.

I am deeply grateful to my parents and sister for their unwavering support and encouragement throughout my journey. Their belief in me has been my foundation, and I couldn't have reached this point without them. I also extend a heartfelt thank you to my partner, Kimiya, whose optimism and support have been crucial during the toughest times, helping me stay focused and positive.

A special thanks to my supervisor, Professor Javad Dargahi, for giving me the opportunity of a lifetime to work with a fantastic team in an amazing environment.

I also want to express my sincere appreciation to my co-supervisor and mentor, Dr. Amir Hooshidar, for his constant support and invaluable advice throughout my research, which were crucial not only in navigating the complexities of my project but also for imparting life lessons that have shaped my personal and professional growth. Finally, I would like to appreciate the amazing team at the SuPER lab especially Amir Sayadi and Andrew Ramos for their guidance and assistance. In addition Aiden, Erfan, Nima, Sarvin, Sepehr, Frank, Marc, Michelle, Helene and others are among the colleagues and friends who have made this journey enjoyable and less stressful.

# Contents

<b>List of Figures</b>	<b>vii</b>
<b>List of Tables</b>	<b>viii</b>
<b>1 Introduction</b>	<b>1</b>
1.1 Background . . . . .	1
1.2 Related studies . . . . .	4
1.3 Motivations . . . . .	8
1.4 Research Objectives . . . . .	8
1.5 Thesis layout . . . . .	8
1.6 Contributions . . . . .	10
<b>2 TransLeNet: Transfer Neural Calibration for Embedded Sensing in Soft Robots</b>	<b>11</b>
2.1 Background . . . . .	11
2.2 Materials and Methods . . . . .	14
2.2.1 Sensor Design and Working Principle . . . . .	14
2.2.2 Experimental Setup and Data Acquisition . . . . .	16
2.2.3 Data Transformation . . . . .	16
2.2.4 Transfer Learning Calibration . . . . .	18
2.2.5 Validation Protocol . . . . .	21
2.3 Results and Discussion . . . . .	21
2.4 Summary . . . . .	26

<b>3</b>	<b>Embedded Force Sensor for Soft Robots With Deep Transformation Calibration</b>	<b>27</b>
3.1	Background . . . . .	27
3.2	Sensor Design and Working Principle . . . . .	29
3.2.1	Modeling and Fabrication . . . . .	29
3.2.2	Experimental Setup and Data Acquisition . . . . .	32
3.2.3	Data Transformation . . . . .	34
3.2.4	Transfer Learning Calibration . . . . .	35
3.2.5	Training Dataset . . . . .	37
3.2.6	Validation Protocol . . . . .	38
3.3	Results and Discussion . . . . .	40
3.3.1	Calibration Verification . . . . .	40
3.3.2	Experimental Validation . . . . .	40
3.4	Summary . . . . .	45
<b>4</b>	<b>Conclusions and Future Works</b>	<b>46</b>
4.1	Conclusions . . . . .	46
4.2	Future Works . . . . .	47
	<b>Bibliography</b>	<b>48</b>

# List of Figures

Figure 1.1	Concept application of soft robots in force-sensitive surgical procedures. . .	3
Figure 2.1	Conceptual application of the soft sensor in cardiovascular procedures. . . .	12
Figure 2.2	Time-frequency analysis of a signal for CQT and STFT . . . . .	13
Figure 2.3	The structural design of the sensor . . . . .	15
Figure 2.4	The fabricated sensor and flexural robot prototype for the experimental setup	17
Figure 2.5	Dataflow-gram of the proposed transfer-learning-based calibration method. .	20
Figure 2.6	Representative performance of the calibration in the $x$ axis. . . . .	23
Figure 2.7	Comparison of estimated and reference forces between transformations . . .	25
Figure 3.1	Comparison of continuous wavelet transforms in Time-Frequency Domain .	28
Figure 3.2	Fabrication process of the soft sensor. . . . .	30
Figure 3.3	The structural design a simplified electrical model of the sensor . . . . .	31
Figure 3.4	The experimental setup for the data acquisition . . . . .	33
Figure 3.5	Dataflow-gram of the proposed transfer-learning-based calibration method. .	36
Figure 3.6	Calibration model training progress. . . . .	39
Figure 3.7	Comparison of estimation and reference forces for all the transformations .	41
Figure 3.8	Comparison of reference forces and estimated forces with Morse transform .	43

# List of Tables

Table 1.1	Comparison of flexible piezo-resistive soft sensors . . . . .	5
Table 1.2	Neural network approaches for soft sensor calibration and their advantages . . . . .	7
Table 2.1	Performance of the calibration in comparison with Ref. [1]. . . . .	23
Table 2.2	Performance metrics for the proposed transformations. . . . .	24
Table 3.1	Composition and contents of the fabricated gelatin-based sensor . . . . .	32
Table 3.2	Performance metrics based on transformations and degrees of freedom . . . . .	42
Table 3.3	Calibration performance compared to other representative studies . . . . .	44

# Chapter 1

## Introduction

### 1.1 Background

Minimally invasive surgery (MIS) has gained significant attention due to its potential advantages over traditional open surgery. Studies show that MIS offers benefits such as reduced operative trauma, faster recovery times, and better cosmetic outcomes [2, 3, 4, 5, 6]. MIS can be performed through endoluminal tissues, through the body's natural orifices or small incisions to access the body's lumens. As shown in Fig. 1.1, flexible surgical instruments are essential for endoluminal navigation, as they enable precise control, navigation, and contact-force estimation during endoluminal surgeries [7, 8]. The flexible nature of these instruments allows for spatial flexibility and dexterity, making endoluminal surgery faster and safer compared to conventional minimally invasive interventions with rigid instruments [9]. Therefore, the development and advancement of soft robots for surgical procedures have been crucial in ensuring instrumental flexibility for safe access and navigation to lesions over long distances in endoluminal and intravascular procedures [7, 8].

Force sensing in the range of 0 to 2N is crucial in MIS procedures such as bronchoscopy and cardiac surgeries where force sensing is constrained, posing challenges to optimal recovery and surgical precision [10, 11]. In cardiac surgery, force sensing is crucial for interventional procedures, demonstrating the effectiveness and potential of robotic systems[12, 1]. Studies demonstrate a lack

of proper force-displacement synchronization in telerobotic surgical systems which can lead to significant motion-tracking error [13, 14]. In addition, soft robots have exhibited excellent compatibility with functional and physical requirements of intraluminal procedures, such as bronchoscopy and cardiovascular interventions [15, 3].

The development of force sensing capabilities has been a focus, with studies proposing algorithms and new instruments with force sensing capabilities to enhance surgical precision and safety [10, 11, 16]. Additionally, the loss of haptic feedback in minimally invasive surgery due to resistance inside trocars and the use of long laparoscopic instruments hinders the estimation of applied forces in instrument–tissue interaction, highlighting the importance of force sensing in these procedures [17]. Moreover, the development of force detection and feedback control for follower manipulators has been identified as critical to the operation, emphasizing the significance of force sensing in surgical robotics [18, 19, 20, 21, 22, 23, 24, 25]. Traditional force sensors such as piezoelectric, piezoresistive, and optical sensors play a crucial role in various applications, including force impact sensing, microscale force measurement, and robotic surgery. Piezoelectric sensors, which generate an electric charge in response to applied mechanical stress, are widely used due to their high sensitivity and ease of integration. For example, piezoelectric sensors have been integrated into smart glass applications to monitor force impact, with a response range reaching up to 10 kPa [26]. Additionally, piezoelectric sensors have been utilized in microscale applications, offering advantages such as low power dissipation and high sensitivity [27]. Piezoresistive sensing materials have been popular due to their ease of development, low cost, and electronic readout [28, 29]. These sensors change their electrical resistance when subjected to mechanical stress, making them suitable for force, displacement, and chemical sensing. Furthermore, piezoresistive sensors have been prototyped for microscale applications, offering high measurement dynamics and easy integration [30]. Optical sensors, including fibre Bragg grating-based sensors, offer high resolution and accuracy for force measurement. These sensors have been used in various applications, such as high-voltage sensing and dynamic scanning force microscopy [31]. In addition, carbon-nanotube-coated 3D microspring force sensors have been developed for medical applications, providing advantages over other tactile force sensors based on film-type polymer-based materials or MEMS structures [32, 33]. On the other hand, optimal mechanical compliance, scalability design, and proper integration of miniature

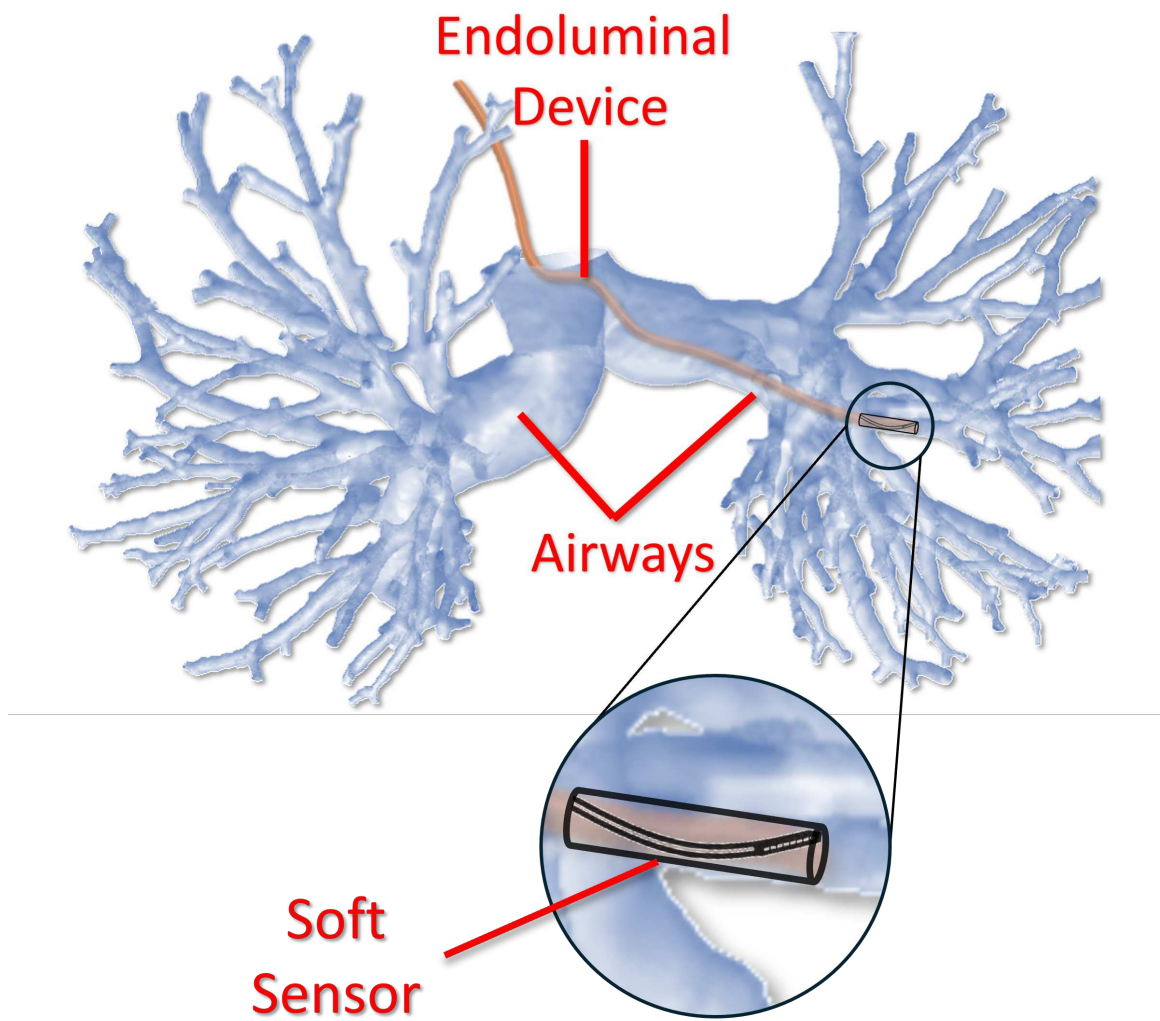


Figure 1.1: Concept application of soft robots in force-sensitive surgical procedures.

rigid force sensors on soft robots are still cumbersome [2]. Despite their superior performance, integrating rigid sensors with soft robots is challenging and they provide limited information only about the installation site. Thus, embedded distributed sensors that are easy to integrate and provide information about the length of the robot are technically needed and of utmost importance for force-sensitive applications, such as endoluminal surgery. In addition, large mechanical deformation of soft robots (i.e. flexures) may push measurements out of sensors' linear range [3], and calibration or characterization of soft sensors beyond their linear response has been minimally explored.

## 1.2 Related studies

Flexible soft sensors have been developed with various materials and sensing capabilities, and one major factor of interest in their fabrication is the flexibility of the sensing material, as this characteristic can widely impact the range, stability, and usability of the sensor. In a previous research, a novel sensing method with soft sensors embedded in flexures was introduced, exhibiting less than 10mN error in measuring external 3D tip forces for bronchoscopy and cardiovascular applications [34]. This flexible sensor comprised a gelatin-based matrix filled with graphite nano-particles that exhibited stable piezoresistivity under extensive deformations. It was shape-agnostic but presented viscoelastic properties[35]. Soft sensors present a high complexity of their piezoresistivity and large intrinsic deformation of the sensing elements, and they are often calibrated based on rate-dependent features, i.e. the rate of change in output voltage for a given input [36]. To compensate for their non-linear behaviours, a proper calibration method is needed. Machine learning techniques have shown the potential to address many challenging problems with nonlinear behaviours [37], such as multi-layer perceptron (MLP) models. However, the accuracy of sensors is adversely affected in noisy environments, e.g. near robotic devices or in clinical operation rooms, where rate-dependent features and neural calibrations amplify electromagnetic interference, decreasing the signal-to-noise ratio [1].

Table 1.1: Comparison of flexible piezo-resistive soft sensors

Study	Functional Material	Range	Sensitivity
Cassa <i>et al.</i> [28] (2022)	PDMS / PEDOT:PSS	0 - 12 N	$\Delta R/R_0 = 70\%$
Wang <i>et al.</i> [38] (2016)	PDMS / MWCNT	0 - 2.51 mN / 0 - 62.8 mN	$-1.10 \text{ kPa}^{-1}$
Ma <i>et al.</i> [39] (2017)	MXenes	0 - 750 mN	Gauge Factor $\sim 180.1$
Xu <i>et al.</i> [40] (2018)	3D graphene	66 kPa	Gauge Factor $\sim 584.2$
Liu <i>et al.</i> [41] (2017)	Graphene / TPU	0 - 100 kPa / 100 - 400 kPa	Gauge Factors $\sim 2.45 / 12.24$
Jia <i>et al.</i> [42] (2019)	Graphene oxide (rGO)	42–3000 Pa	$7.94 - 178.1 \text{ kPa}^{-1}$
Radó <i>et al.</i> [43] (2018)	Si / PDMS	0.01 - 2 N	Loss: $\pm 3 \pm 10\% \Delta V / \Delta F$
Zhao <i>et al.</i> [44] (2019)	HPM / PDMS	$\leq 140 \text{ Pa}$	$83.9 \text{ kPa}^{-1}$
Lim <i>et al.</i> [45] (2019)	AgNWs	20% of strain	-
Hessinger <i>et al.</i> [46] (2016)	Si	1 mN - 10 N	-

Researchers have used machine learning techniques for soft sensor calibration. Kim *et al.*[47, 48] applied various methods for contact localization and force estimation of soft sensors: one being a simple artificial neural network composed of two fully connected layers of 25 and 12 hidden nodes, another was a supervised-learning method based on K-Nearest Neighbours (K-NN), a third approach was logic combinations, and their last method was a Recurrent Neural Network (RNN). Their results show that the RNN was the best for contact localization and force estimation. However, their latest approach included a Time-Delay Artificial Neural Network (TDNN) for fast online calibration. In another study, Han *et al.*[49] investigated a deep learning method for characterizing soft sensors. They also applied an RNN for contact localization and force estimation and achieved over 93.2% accuracy (above 100 kPa) on every sensor's part. Since large data collection has been a concern, Kim *et al.* investigated a new approach for calibrating soft sensors using transfer learning techniques. These deep learning methods reduced data size by 25%, decreasing processing time and computational cost. They also implemented pre-trained networks to address these issues and were able to apply this method for long-term sensor use [48]. The previous and current work includes Deep Convolutional Neural Network (DCNN). Table 1.2 compares these approaches to soft sensor calibration.

Table 1.2: Neural network approaches for soft sensor calibration and their advantages

<b>Study</b>	<b>Type of Neural Network</b>	<b>Advantages</b>
Han <i>et al.</i> [49] (2018)	RNN	Contact Localization Force Estimation
Kim <i>et al.</i> [47] (2018)	RNN	Contact Localization Force Estimation
Kim <i>et al.</i> [48] (2020)	TDANN	Contact localization Force Estimation Nonlinearity Compensation Hysteresis Compensation Pre-trained Online Estimation
Torkaman <i>et al.</i> [1] (2023)	MLP	Contact Localization Force Estimation Nonlinearity Compensation Hysteresis Compensation
Masoumi <i>et al.</i> [50] (2023)	DCNN	Contact Localization Force Estimation Nonlinearity Compensation Hysteresis Compensation Online Estimation Pre-trained
Masoumi <i>et al.</i> [51, 52] (2024)	DCNN	Contact Localization Force Estimation Nonlinearity Compensation Hysteresis Compensation Online Estimation Pre-trained Noiseless

**RNN:** Recurrent Neural Network  
**TDANN:** Time-Delay Artificial Neural Network  
**MLP:** Multi-Layer Perceptron  
**DCNN:** Deep Convolutional Neural Network

### **1.3 Motivations**

Researchers have tried to use soft embedded sensing for real-time status awareness in intraluminal interventions. However, technical challenges such as hysteresis, rate-dependency, and viscoelasticity of sensing elements have limited the accuracy and usability of such embedded sensors. In this thesis, the main motivation was to eliminate the need for derivation-based features to compute temporal effects such as hysteresis and rate-dependency and to propose a calibration framework to use those derivative-free time-frequency features in soft force sensing.

### **1.4 Research Objectives**

To address the identified knowledge gaps outlined in Section 1.3, the specific aims of this study were:

- (1) To investigate the feasibility of using computational signal transformers, such as Wavelets as calibration features for soft sensors,
- (2) To investigate the performance of pre-trained deep neural net transformers such as LeNet for pattern recognition and calibration of soft sensors based on derivative-free time-frequency transformation features,
- (3) To compare performance of soft sensor calibration based on derivative-free time-frequency transformations.

### **1.5 Thesis layout**

This thesis is prepared in manuscript-based style according to the "Thesis Preparation and Thesis Examination Regulations (version-2022) for Manuscript-based Thesis" of the School of Graduate Studies of Concordia University. This dissertation includes four chapters with the following contents:

Chapter 1 presents the results of a critical literature review of force and shape sensors for soft robots with regard to the state-of-the-art modeling approaches, methods, and knowledge gaps.

Chapter 2 presents the design, modeling, calibration and signal processing of the sensor using two transformations. This chapter is based on the author's following publications:

- (1) Masoumi, Navid, Negar Kazemipour, Sarvin Ghiasi, Tannaz Torkaman, Amir Sayadi, Javad Dargahi, and Amir Hooshiar. "WaveLeNet: Transfer Neural Calibration for Embedded Sensing in Soft Robots." (No. 10507) [50]
- (2) Masoumi, Navid, Andres C. Ramos, Tannaz Torkaman, Javad Dargahi, Jake Barralet, Liane S. Feldman, and Amir Hooshiar. "Embedded Force Sensor with Deep Transformation Calibration for Interventional Soft Robots." In 2024 46th Annual International Conference of the IEEE Engineering in Medicine and Biology Society (EMBC), pp. 1-4. IEEE, 2024. [52]

The author's contribution was primarily in the data pre-processing, machine learning developments, post processing, interpretation, and drafting. The contribution of the second author was in prototyping and initial data acquisition. The contribution of the third and fourth authors were in data pre-processing, data acquisition and drafting. The contribution of the sixth to ninth authors were in supervision, funding, final drafting and review.

Chapter 3 reports the implementation and comparison of performance for the proposed calibration method with six different temporal-frequency signal transformers. This chapter was drafted based on the following manuscript:

- (1) Masoumi, Navid, Andrés C. Ramos, Tannaz Torkaman, Liane S. Feldman, Jake Barralet, Javad Dargahi, and Amir Hooshiar. "Embedded Force Sensor for Soft Robots With Deep Transformation Calibration." IEEE Transactions on Medical Robotics and Bionics (2024). [51]

The main contribution of the author was in data pre-processing, machine learning developments, post-processing, interpretation, and drafting. The second author's contribution involved prototyping and initial data acquisition. The contributions of the third and fourth authors included data pre-processing, data acquisition, and drafting. Contributions from the sixth to ninth authors encompassed supervision, funding, final drafting, and review.

## 1.6 Contributions

This study was, to the best of the author’s knowledge, the first to address the limits of rate-dependent calibration methods for embedded soft sensors for the application of interventional soft robots, by proposing an innovative approach to have a derivative-free, transfer learning-based calibration approach that minimizes noise amplification and improves precision in the measurement of subtle forces, particularly in the mentioned applications requiring high sensitivity at low force ranges.

The results of this research have been published as two conference papers and a journal paper:

- (1) Masoumi, Navid, Negar Kazemipour, Sarvin Ghiasi, Tannaz Torkaman, Amir Sayadi, Javad Dargahi, and Amir Hooshidar. "WaveLeNet: Transfer Neural Calibration for Embedded Sensing in Soft Robots." (No. 10507)
- (2) Masoumi, Navid, Andres C. Ramos, Tannaz Torkaman, Javad Dargahi, Jake Barralet, Liane S. Feldman, and Amir Hooshidar. "Embedded Force Sensor with Deep Transformation Calibration for Interventional Soft Robots." In 2024 46th Annual International Conference of the IEEE Engineering in Medicine and Biology Society (EMBC), pp. 1-4. IEEE, 2024
- (3) Masoumi, Navid, Andrés C. Ramos, Tannaz Torkaman, Liane S. Feldman, Jake Barralet, Javad Dargahi, and Amir Hooshidar. "Embedded Force Sensor for Soft Robots With Deep Transformation Calibration." IEEE Transactions on Medical Robotics and Bionics (2024)

## Chapter 2

# TransLeNet: Transfer Neural Calibration for Embedded Sensing in Soft Robots

### 2.1 Background

Soft robots have exhibited excellent compatibility with functional and physical requirements of intraluminal procedures such as bronchoscopy and cardiovascular intervention [15, 53]. Despite their favourable mechanical compliance and scalable design, integrating miniature force and shape sensors on them is cumbersome [2]. Also, large mechanical deformation of such robots, i.e., flexures, may push traditional rigid sensors out of their linear range [3]. As an alternative approach, a previous study have introduced a novel soft sensing method and soft embedded sensors for flexures that exhibited less than 10mN error in measuring external 3D tip forces on soft robots for bronchoscopy and cardiovascular applications [34, 1]. Fig. 2.1 depict a representative interventional application. The proposed soft sensor was comprised of a gelatin-based matrix filled with graphite nano-particles that exhibited stable piezoresistivity under extremely large deformation. Despite its accuracy, the accuracy of the proposed sensor was adversely affected in noisy environments, e.g., operation rooms. The reason was that the rate-dependent features used in its neural calibration

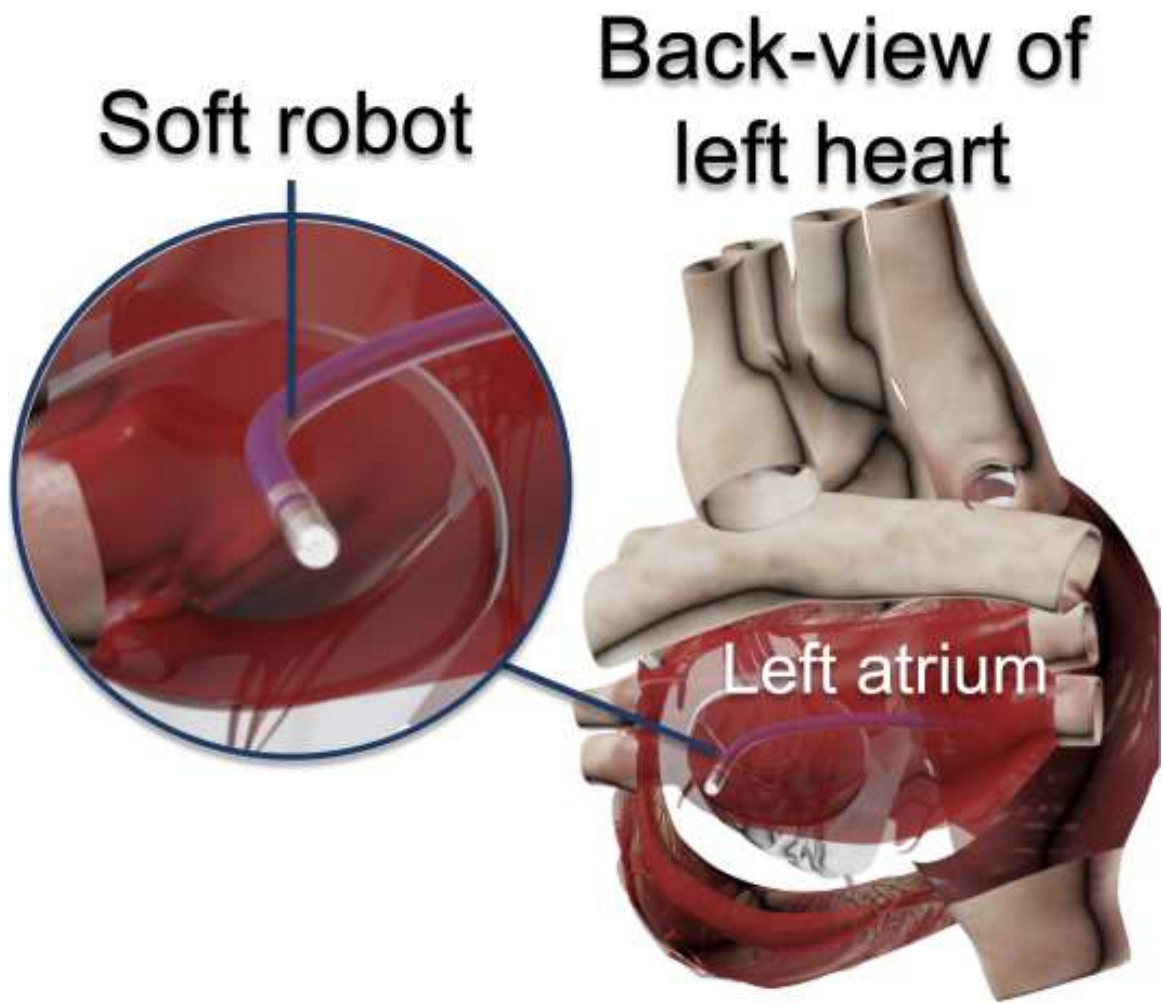


Figure 2.1: Conceptual application of the proposed soft sensor in cardiovascular procedures.[35]

would amplify the peripheral noise which would diminish the accuracy. In this chapter, an alternative deep-learning-based method is proposed and validated for calibration of the mentioned soft sensor that is derivative-free thus does not amplify the peripheral noise and is versatile. Conceptually, the proposed calibration methods can be used to assemble an array of sensor readings for distributed sensing on soft robots. The proposed method is based on generating a scalogram from the temporal-frequency content of the measured voltages using real-time transforms such as Short-Time Fourier and Constant-Q and using transfer learning technique to infer rate-dependent and deformation-dependent features from the voltages' scalogram.

The STFT, introduced by Dennis Gabor, operates by segmenting a signal into overlapping frames and applying the Fourier Transform to each frame. This method provides a time-frequency representation that captures both temporal and spectral information, making it suitable for analyzing non-stationary signals [18]. However, the STFT is limited by its fixed window size, which can lead to a trade-off between time and frequency resolution. A larger window provides better frequency resolution but poorer time resolution, while a smaller window offers the opposite [54, 55]. This limitation has prompted the development of adaptive techniques, such as the Adaptive Short-Time Fourier Transform (ASTFT), which adjusts the window size based on local signal characteristics, albeit at the cost of increased computational complexity [54, 56].

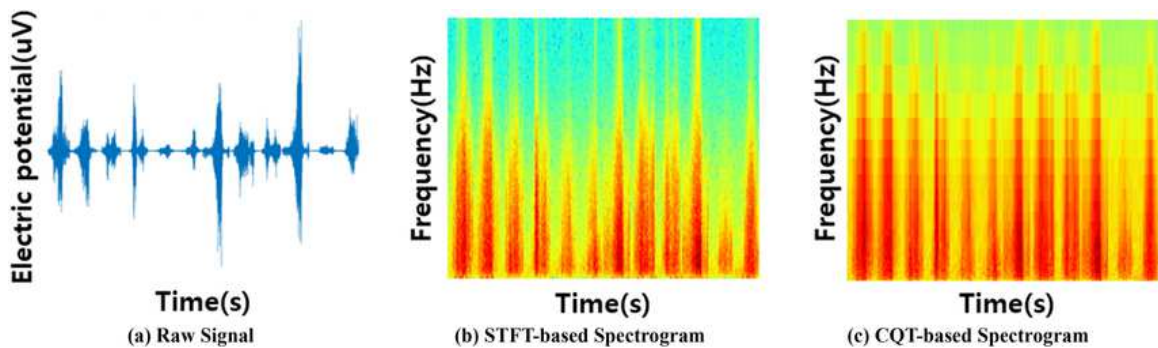


Figure 2.2: Time-frequency analysis of a signal in a representative study [57] using STFT and CQT, demonstrating differences in frequency resolution.

In contrast, the Constant-Q Transform (CQT) is designed to provide a frequency resolution that is proportional to the frequency itself, which is particularly advantageous for musical and audio signals where lower frequencies require higher resolution [58]. The CQT uses logarithmically spaced

frequency bins, allowing it to maintain a consistent quality factor ( $Q$ ) across the frequency spectrum. This characteristic makes the CQT especially effective for applications in music information retrieval and audio analysis, where the perception of pitch and harmonic content is crucial [59]. Additionally, the CQT can be computationally intensive due to its non-uniform frequency sampling, but it offers superior performance in scenarios where frequency resolution is paramount [60]. Fig. 2.2 illustrates a comparative analysis of STFT and CQT to elucidate the distinct frequency resolution characteristics of these transformations.

## 2.2 Materials and Methods

### 2.2.1 Sensor Design and Working Principle

In a recent research, a novel soft sensing method with soft sensors embedded in flexures was introduced, exhibiting less than 10mN error in measuring external 3D tip forces for bronchoscopy and cardiovascular applications [34]. As shown in Fig. 2.3, the sensor was composed of gelatin-based matrix filled with graphite nano-particles with piezoresistive properties [35]. The schematic shows the electrode wiring inside the sensing element's flexure and a streamlined equivalent electrical model of the sensor's voltage-splitting setup for data collection. The voltage  $V_2$  and resistance  $R_e$  represent the voltage at the sensor tip and the sensing element's total electrical resistance. Moreover,  $R_c$  is a constant resistor required for voltage splitting, and  $V_1$  is the pull-up voltage used to trigger the voltage splitter circuit. The electrical resistance of the gelatin and graphite composites change when they deform due to their piezoresistive properties. This behaviour results from variations in the effective diameter and length of the sensing element within the soft body caused by deformation due to external excitation, which can be generated by applying force or pressure on the soft sensor. As shown in Fig. 2.3, the helically shaped force sensor, with three degrees of freedom of detection, is positioned along the cylindrical chamber in the flexural body. Such chambers also function as a mold for the suggested gelatin-based sensing element. To produce the soft body, a 3D printer and PLA filaments (Replicator+, MakerBot, NY, USA) were used to make cylindrical molds that hold the sensing material in place. Ecoflex 00-50 was combined in a 1 to 1 ratio, stirred for 5 minutes, and then allowed to degas under a vacuum of 101 kPa. After being injected into the molds,

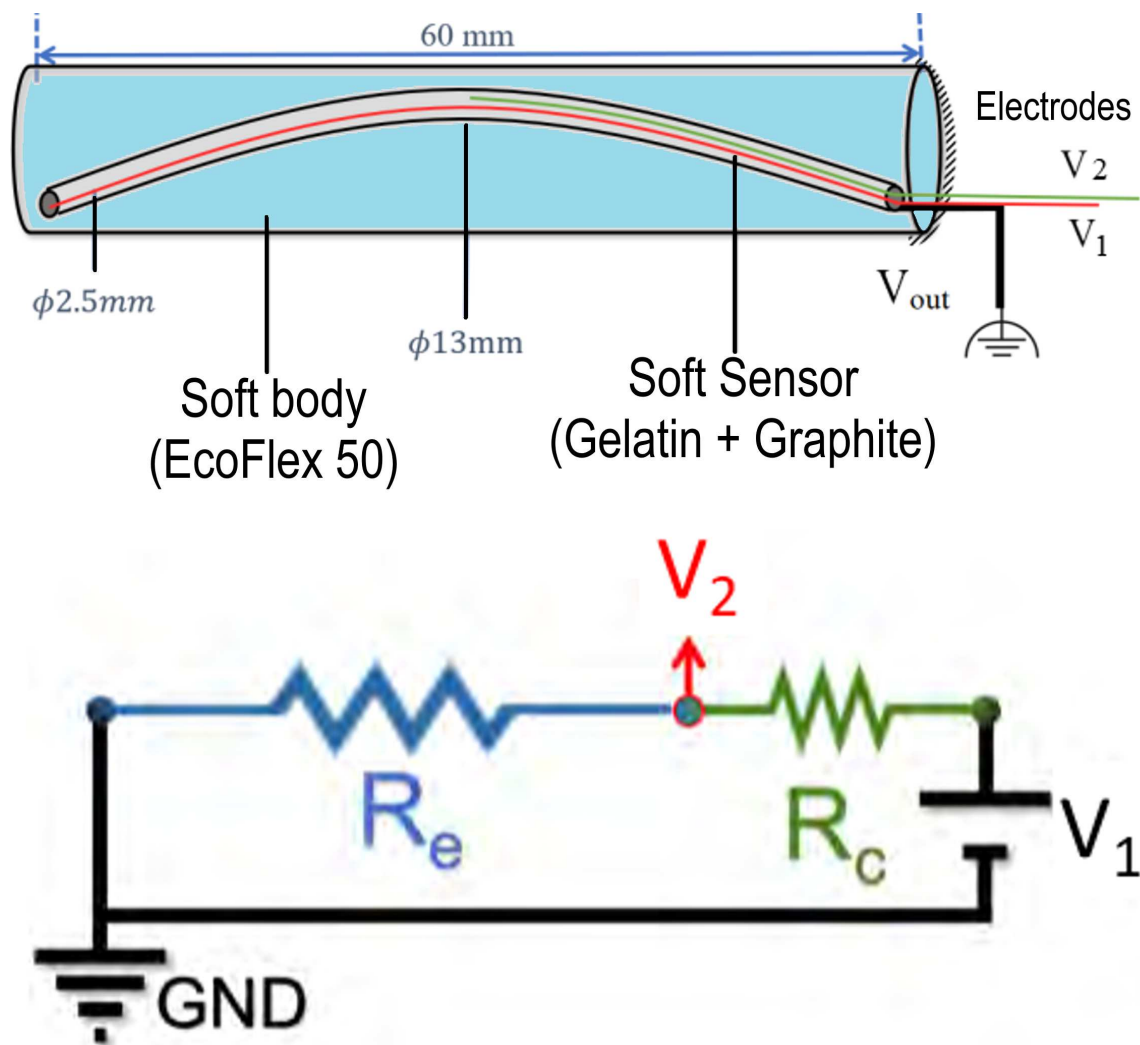


Figure 2.3: Top: the structural design of the sensor with a gelatin/graphite sensing element. Bottom: simplified electrical model of the sensor and voltage splitter circuit.

the mixture was allowed to settle for 24 hours at 25°C. The sensing component was fabricated by incorporating graphite micro platelets into the gelatin. The gelatin sachets were dissolved by stirring them after being immersed in cold water for two minutes. This emulsion was injected into the chamber of the soft body, after mixing it with graphite micro platelets.

## 2.2.2 Experimental Setup and Data Acquisition

Fig. 2.4 depicts the fabricated flexural robot with the embedded sensing element and the experimental validated setup used in this study[34], consisting of a Gamma force and torque sensor (ATI Industrial Automation, NC, USA) to measure the ground truth force values acting on the flexural robot and sensing element. An Arduino Uno was used to measure  $V_1$  and  $V_2$  raw data at a 250 Hz refresh rate and transfer the data to a PC. A user interface software for data acquisition, curation, storage, and post-processing was developed in C# programming language, integrating the software on the PC, the firmware on Arduino Uno, and the hardware (sensor and flexure). The data post-processing and calibration were performed in Matlab 2023a (Mathworks, MA, USA).

## 2.2.3 Data Transformation

Data is comprised of two sets of voltage signals, namely  $z(t)$  hereinafter, collected over time. In a previous research[1], such voltage signals were kept in the time domain and fed to a neural network, so no information containing frequency components was processed. However, the focus in this study is to enhance the calibration process by considering the features in the frequency domain while the temporal data is still being processed. For extracting such frequency components from the voltage signals in the form of a time series, two types of transforms are implemented. The first approach is a short-time Fourier transform (STFT) which represents a sort of trade-off between time and frequency-based views of a signal with limited accuracy, where the size of the frames determines that accuracy. These functions were studied to find the best candidates for input data that achieve the best regression results. The STFT is based on the fundamental continuous form[61] as defined in Eq. 4.

$$Z(\tau, w) = \int_{-\infty}^{\infty} z(t)w(t - \tau)e^{-iwt} dt \quad (1)$$

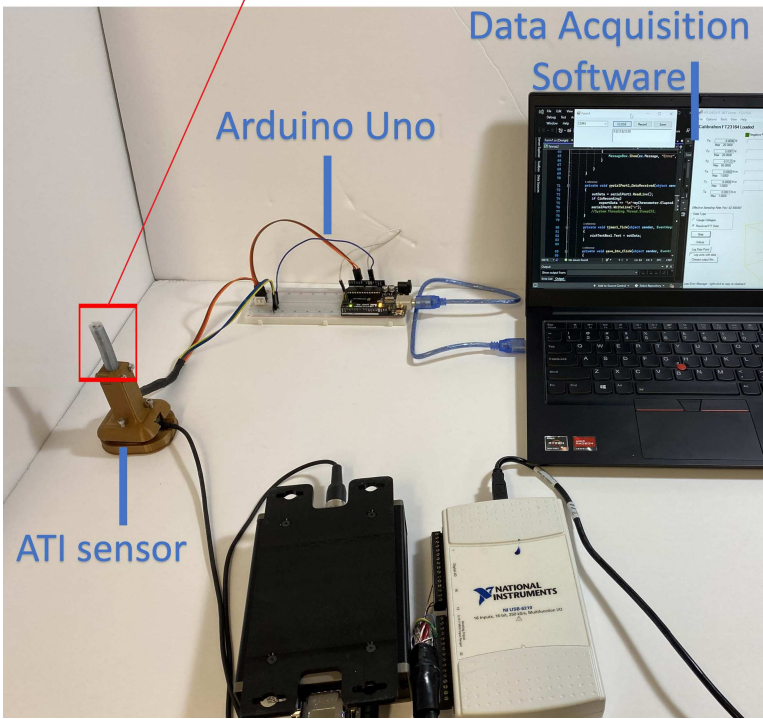
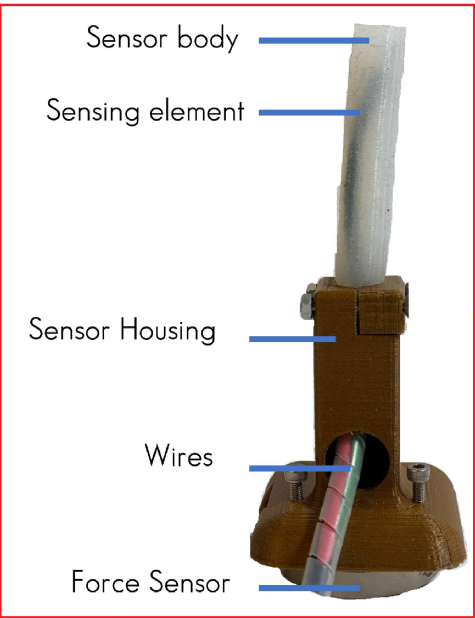


Figure 2.4: The fabricated sensor and flexural robot prototype, and the experimental setup used in data acquisition of this study.

where  $z(t)$  denotes the original signal which is being investigated, while  $Z(\tau, w)$  represents the outcome of applying the STFT at a specific time window function of  $\tau$ . The second approach is based on a Constant-Q Transform that is intuitive for time-frequency analysis. The ratio of the filter's center frequency to bandwidth is known as the "Q factor", indicating the selectivity of a filter when used in time-frequency analysis. It can be defined as in Eq. 2:

$$Q = \frac{f_k}{f_{k+1} - f_k} \quad (2)$$

where  $k = 1, 2, \dots, K$  is the frequency bin index and  $f_k$  is the centre frequency of bin  $k$  [62]. The CQT has an optimal temporal resolution for higher frequencies but a larger frequency resolution at lower frequencies when compared to the STFT. The CQT of a discrete signal  $x(n)$  is as found in Eq. 3:

$$X^{CQ}(k, n) = \sum_{j=n-\lfloor N_k/2 \rfloor}^{n+\lfloor N_k/2 \rfloor} x(j) a_k^*(j - n + N_k/2) \quad (3)$$

where  $a_k(n)$  are basis functions,  $*$  is the complex conjugate, and  $N_k$  is a variable window length [62].

## 2.2.4 Transfer Learning Calibration

As an alternative and derivative-free calibration method for the soft embedded sensor developed in [1], the utilization of a deep-learning-based calibration schema is investigated. To this end, first the transformation scalograms of two voltages  $V_1$  and  $V_2$  recorded during the sensor calibration were obtained using Matlab Signal Processing Toolbox. As shown in Fig. 2.5 scalograms were 2D images in red-green-blue (RGB) colorspace. The images were of  $224 \times 112$  px size and were horizontally concatenated in the form of  $[V_1 V_2]$  to form a  $224 \times 224$  px input image for the transferred neural network. Also, the synchro-squeezing, which is a signal processing technique that improve the clarity and accuracy of time-frequency analyses, was utilized to refine the temporal resolution of the scalogram. A total of 70 pairs of STFT and CQT scalograms were obtained from the calibration dataset obtained in [1]. Considering the small size of the dataset and to perform accurate feature

extraction on scalogram images, GoogLeNet (Alphabet Inc.) pre-trained network was used. It had a total of 22 layers (including convolutional and max-pooling. To perform force estimation (regression), the last layer of GoogLeNet (classifier) was replaced with eight fully-connected layers with 250,200,150,100,50,25,10, and 3 neurons with the rectified linear unit (ReLU) activation function.

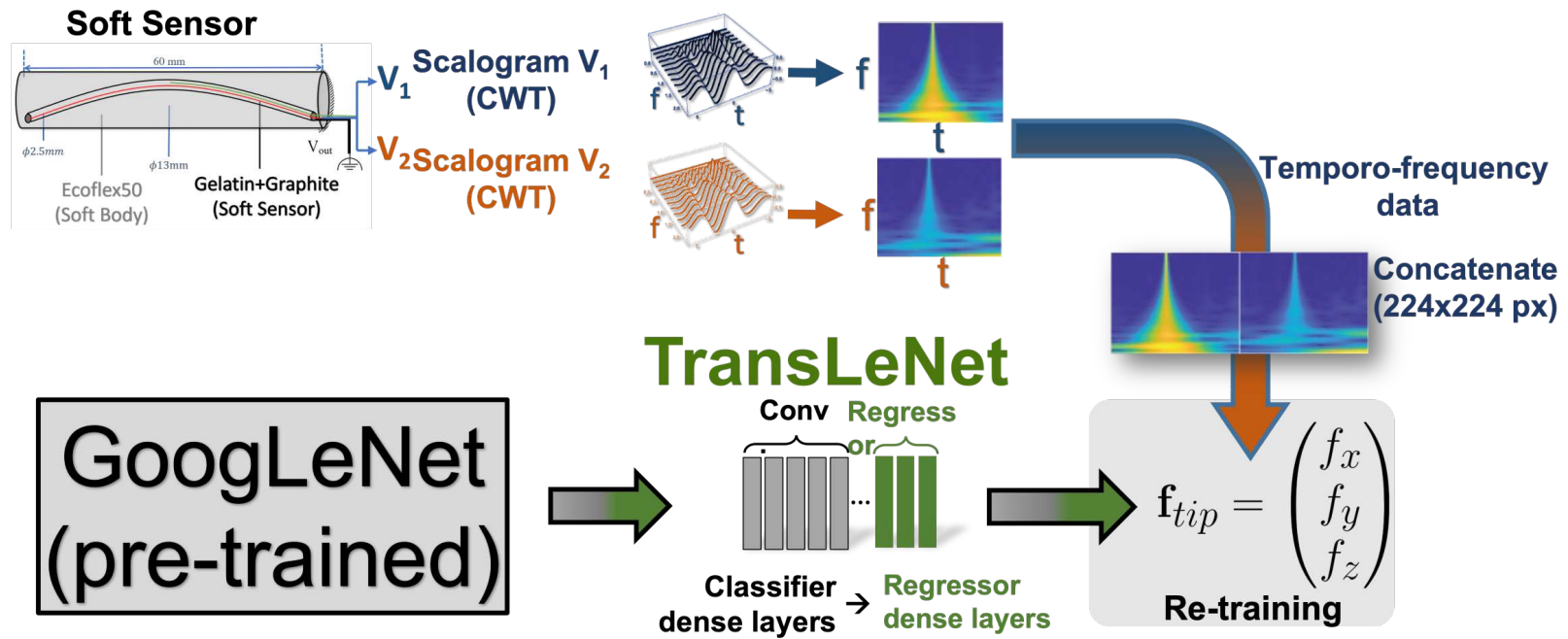


Figure 2.5: Dataflow-graph of the proposed transfer-learning-based calibration method.

The restructured convolutional calibration model was denoted as `TransLeNet` in this study. For better accuracy, the training forces were normalized. In training, 'adam' optimizer with 20 epochs and goal function of mean-absolute error was used. The training was performed in Matlab Deep Learning Tool Box (Mathworks, MA, USA). The dataset was split (70:15:15 for train:validate:test).

### 2.2.5 Validation Protocol

In a different study, forces were predicted by transferring the calibration model to the developed user interface. Concurrently, the ground-truth force measurements of ATI sensor were acquired. As in training evaluation demonstrated in Fig. 2.4, the soft body was manually deformed at its tip throughout the test. Following that, an analysis of the inaccuracy was conducted by comparing the anticipated forces with the actual values. The time variations in the predicted and ground-truth forces in the validation experiment are reported in the results section. In the validation experiment, discrepancies between the predicted forces and the actual measurements were thoroughly analyzed to assess the calibration model's performance. This analysis involved observing the temporal changes between the two sets of forces and evaluating the robustness and reliability of the predictive model under various operational conditions.

## 2.3 Results and Discussion

Fig. 2.6 shows a representative performance of the proposed calibration for unseen data for predicting tip force in  $x$ -direction, i.e.  $F_x$ . To assess the accuracy, maximum and mean absolute errors between predicted force and ground truth (reference) were analyzed and compared with the previous rate-dependent calibration proposed in [1]. In addition, the minimum detectable force observed with `TransLeNet` and that of [1] were compared. Table 2.1 summarizes the performance of `TransLeNet` with the rate-dependent calibration proposed in [1]. The results showed that the Mean Absolute Error (MAE) of the proposed network was less than 5% of full range. Although the MAE over full range was larger than the previous rate-dependent calibration it was still below the 5% error level. Most importantly, the error for small force ranges were analyzed, where the previous

rate-dependent calibration was most erroneous (due to noise amplification). The results showed that not only the proposed TransLeNet calibration was more accurate than the rate-dependent calibration, but it was also more accurate compared to itself at full range. Also, the more in-depth analysis showed that at force ranges  $> 100\text{mN}$ , the scalograms become quite bright and the temporal gradient of WaveLet scalograms diminishes. Based on the observations in accuracy assessment studies of this chapter, the proposed calibration led to lower accuracy at high forces compared to Torkaman *et al.*[1].

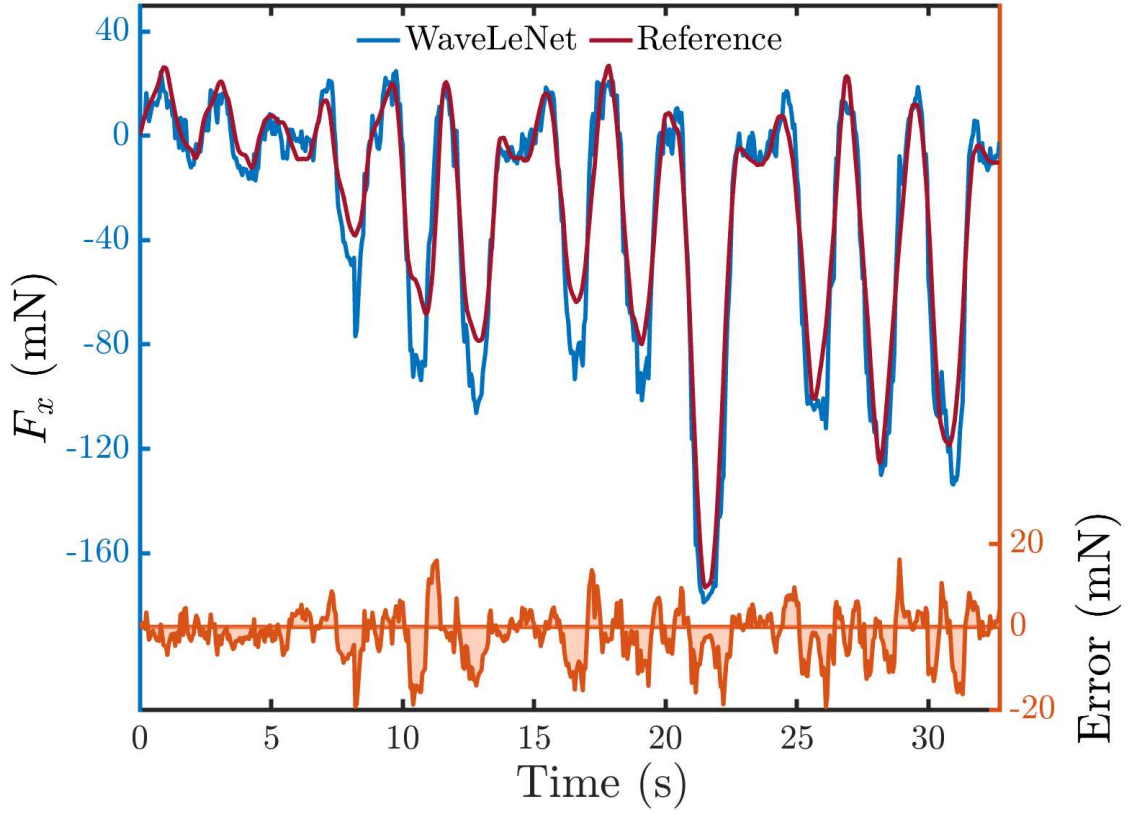


Figure 2.6: Representative performance of the calibration in the  $x$  axis.

Table 2.1: Performance of the calibration in comparison with Ref. [1].

Force	MAE	MAE	MDF	MDF
	TransLeNet (mN)	[1] (mN)	TransLeNet (mN)	[1] (mN)
$F_x$ (full-range)	7.5	3.3	< 1	< 1
$F_y$ (full-range)	7.1	2.6	< 1	< 1
$F_z$ (full-range)	12	8.0	< 1	< 1
$F_x < 20\text{mN}$	3.3	12.0	< 1	< 1
$F_y < 20\text{mN}$	3.7	13.1	< 1	< 1
$F_z < 20\text{mN}$	5.4	14.4	< 1	< 1

MAE: Mean Absolute Error  
MDF: Minimum Detectable Force

The goodness of fit ( $R^2$ ) and Root Mean Squared Error (RMSE) metrics were used to assess TransLeNet’s performance, after 20 epochs and 800 iterations. The  $R^2$  score of the representative transform (CQT) for  $F_x$ ,  $F_y$ , and  $F_z$  was determined to be 92.0%, 97.1%, and 97.0%, respectively, which proves that it is a remarkable fit for the model and target variable. The RMSE, which measures the average squared difference between the predicted and actual values, was 0.346. This means the model has a relatively low error and predicts the target variable well. Overall, as seen by its significant  $R^2$  score and low RMSE, TransLeNet performs high force estimation based on these tests. A performance comparison of the suggested transforms is shown in Fig. 2.7. To this end, we illustrate the calibration method for unseen data from tip force prediction in the X direction, i.e.  $F_x$ . For each transform, the Mean Absolute Error (MAE) and Maximum Absolute Error (MaxAE) of the predicted force are shown in Table 3.2.

Table 2.2: Performance metrics for the proposed transformations.

<b>Transformation</b>	<b>Measurand</b>	<b>Range (mN)</b>	<b>MAE* (mN)</b>	<b>MaxAE** (mN)</b>
CQT	$F_x$	-180 , 260	4.3	25.7
	$F_y$	-140 , 120	2.7	14.2
	$F_z$	-80 , 380	11.2	37.8
STFT	$F_x$	-390 , 210	6.7	39.5
	$F_y$	-350 , 280	5.9	35.0
	$F_z$	-150 , 650	24.1	65.1

\* **MAE:** Mean Absolute Error, \*\* **MaxAE:** Maximum Absolute Error

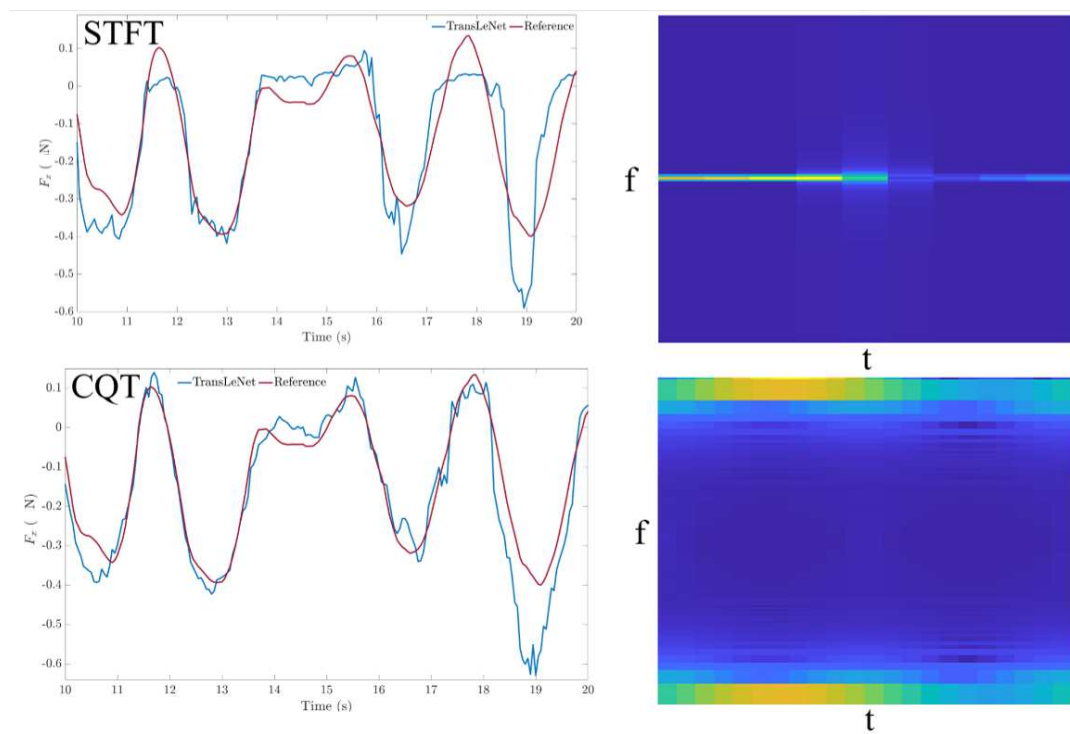
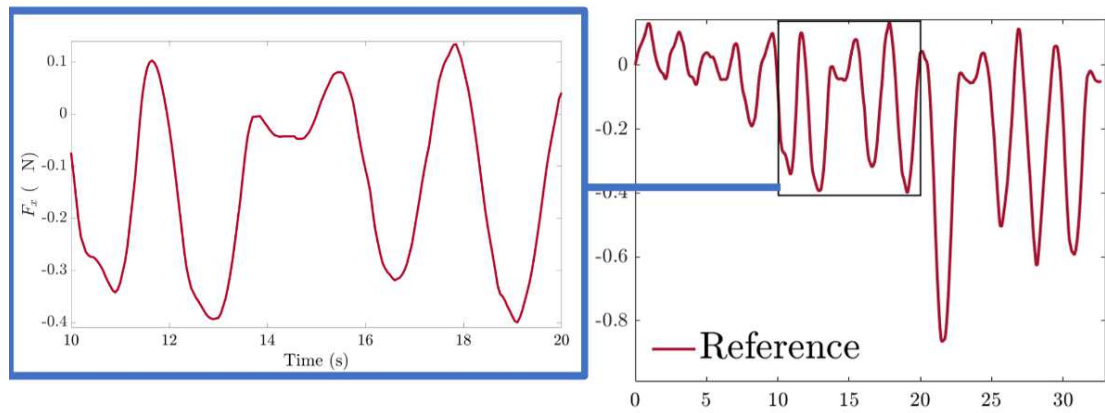


Figure 2.7: Comparison of estimated and reference forces between transformations and their corresponding scalograms.

## 2.4 Summary

A novel calibration method for gelatin-graphite-based soft sensors utilizing convolutional deep learning has been introduced to account for sensor non-linearity and reduce noise. This technique offers improved force sensitivity, particularly beneficial in delicate surgical contexts, with a mean absolute error as low as 11.2 mN. The study underscores the importance of minimally invasive surgery (MIS) and addresses challenges with integrating conventional force sensors in flexible surgical instruments. The proposed embedded and distributed sensors are crucial for accurately sensing interaction forces during procedures like endoluminal surgery. The research introduces 'TransLeNet', an advanced calibration model employing time-frequency signal transformations to refine force estimation in soft sensors. This model incorporates convolutional neural networks and uses transfer learning to improve calibration with limited data. Results showed an excellent fit with an  $R^2$  of over 92% and a low root mean squared error, indicating high accuracy in force estimation. Constant-Q Transform (CQT) provided better results than Short-Time Fourier Transform (STFT) in comparison tests. The study concludes that integrating piezoresistive gelatin-graphite sensors in soft robots offers significant potential for enhancing surgical precision. The use of deep learning in calibration effectively handles non-linearities of such sensors, providing reliable force feedback crucial for surgical success.

## Chapter 3

# Embedded Force Sensor for Soft Robots With Deep Transformation Calibration

### 3.1 Background

Soft shape sensors play a crucial role in enhancing the capabilities of surgical interventional robots by providing real-time feedback on the robot's configuration and interaction with soft tissues. These sensors, often integrated into soft robotic structures, utilize their deformability to capture complex shapes and movements, which is essential in delicate surgical procedures. Calibration methods for these sensors are vital to ensure accurate readings and reliable performance. Various approaches have been proposed, including vision-based calibration techniques that leverage RGB-D cameras to establish the relationship between the robot's coordinate system and the sensor outputs, as demonstrated by Zhang *et al.*[63]. Additionally, kinematic calibration methods, such as those explored by Wei-Dong *et al.*[64], utilize optical position sensors to enhance the precision of surgical robots, ensuring that the robot's movements correspond accurately to the intended actions. Furthermore, the integration of machine learning techniques has been shown to improve calibration processes, allowing for adaptive recalibration in response to changes in the surgical environment or instrument configurations, as discussed by Kim *et al.*[65] and Truby *et al.*[66].

The Continuous Wavelet Transform (CWT) is an effective method for analyzing non-stationary signals by decomposing them into wavelets that are localized in both time and frequency. Among the

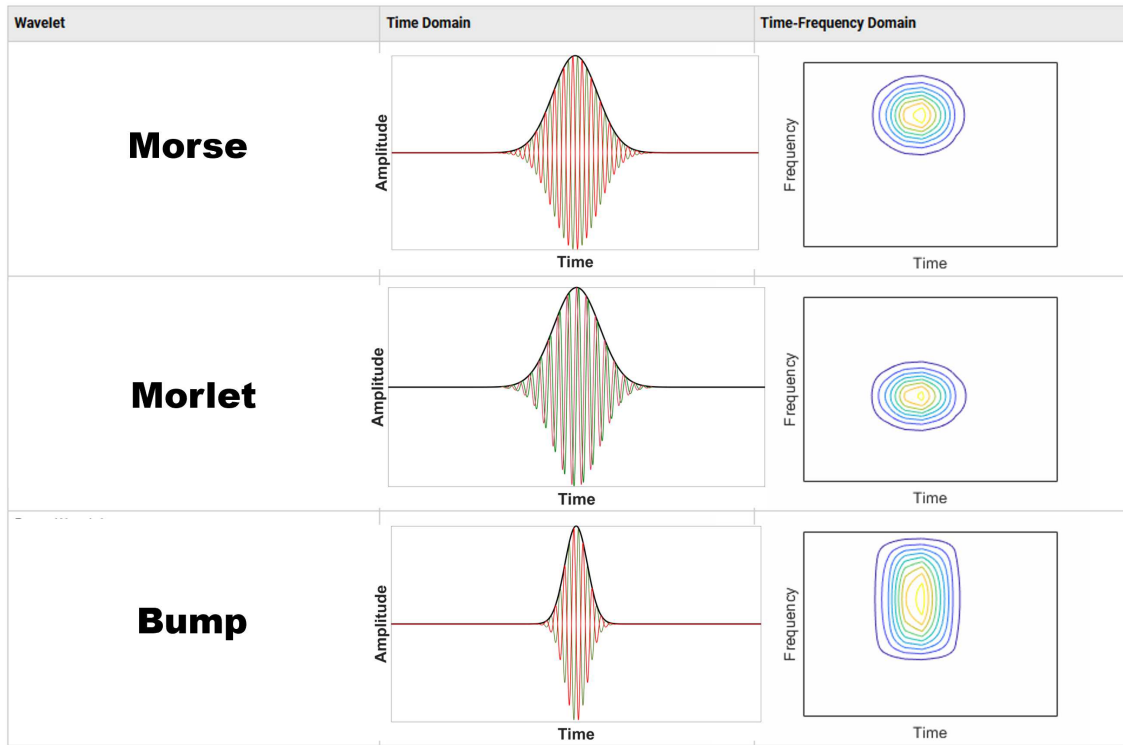


Figure 3.1: Comparison of continuous wavelet transforms in Time-Frequency Domain

various wavelet functions, the Morlet, Morse, and Bump wavelets are particularly noteworthy. The Morlet wavelet, characterized by a Gaussian envelope modulated by a complex sinusoid, is widely used for its balanced time-frequency resolution, making it suitable for applications in seismic signal analysis and mechanical fault detection [67, 68]. The Morse wavelet offers flexibility in its shape, allowing for adjustments in frequency and bandwidth, which is beneficial for analyzing signals with varying frequency content, such as climate data in [69]. Conversely, the Bump wavelet is compactly supported and smooth, making it ideal for localized analysis without introducing artifacts associated with infinite support wavelets [70]. In signal processing and calibration, the choice of wavelet depends on the specific characteristics of the signal; the Morlet wavelet is favored for its resolution, the Morse wavelet for its adaptability, and the Bump wavelet for its localized nature, each enhancing the analysis of complex signals as shown in 3.1.

In this chapter, the process of design and fabrication of the soft sensor in [1] is briefly described. In addition, five transformations (including CQT and STFT from last chapter) are being investigated and compared all together for the neural calibration. The optimal transformation is chosen for the

previously discussed application, based on various metrics such as linearity (R2 score), mean absolute error (MAE), and maximum absolute error (MaxAE). Therefore, an improved and extended calibration architecture, 'TransLeNet' is proposed, to compare a total of five candidates as time-frequency signal transformations, i.e., Morse, Morlet, Bump, Constant Q (CQT), and Short-Time Fourier Transform (STFT), demonstrating their high performance in resolution and range of sensing with the utilized soft sensor and identifying the corresponding best model.

## 3.2 Sensor Design and Working Principle

### 3.2.1 Modeling and Fabrication

The fabrication process of the soft sensor is described in detail in a previous work by Torkaman *et al.*[1]. As shown in Fig. 3.2, the developed soft sensor is built from two merged structures. One is the sensing material, which is based on gelatin and graphite filaments, and the second structure, or soft body, surrounds the sensing elements to provide mechanical support and acts as a flexible vessel sensitive to mechanical deformation. The schematic shows the electrode wiring inside the sensing element's flexure and a streamlined equivalent electrical model of the sensor's voltage-splitting setup for data collection.

$V_1$  represents the voltage at the middle of the sensor,  $V_2$  the voltage at the sensor's tip, and the resistance  $R_e$  represents the sensing element's total electrical resistance. In addition,  $R_c$  is a constant resistor required for voltage splitting, and  $V_{out}$  is the pull-up voltage used to trigger the voltage splitter circuit. The electrical resistance of the gelatin and graphite composites change when they deform due to their piezoresistive properties. This behaviour results from variations in the effective diameter and length of the sensing element within the soft body caused by mechanical deformation due to external forces applied to the soft sensor. For proof of concept, the developed sensor has a diameter that allows practical manipulation and excitation, and thus a calibration process with ease. As shown in Fig. 3.3, the curved force sensing element, with three degrees of freedom of detection, is positioned along the cylindrical chamber in the flexural body. Such a chamber also functions as a mold for the suggested gelatin-based sensing element. For the soft body, a 3D printer and PLA filaments (Replicator+, MakerBot, NY, USA) were used to make cylindrical molds that hold the

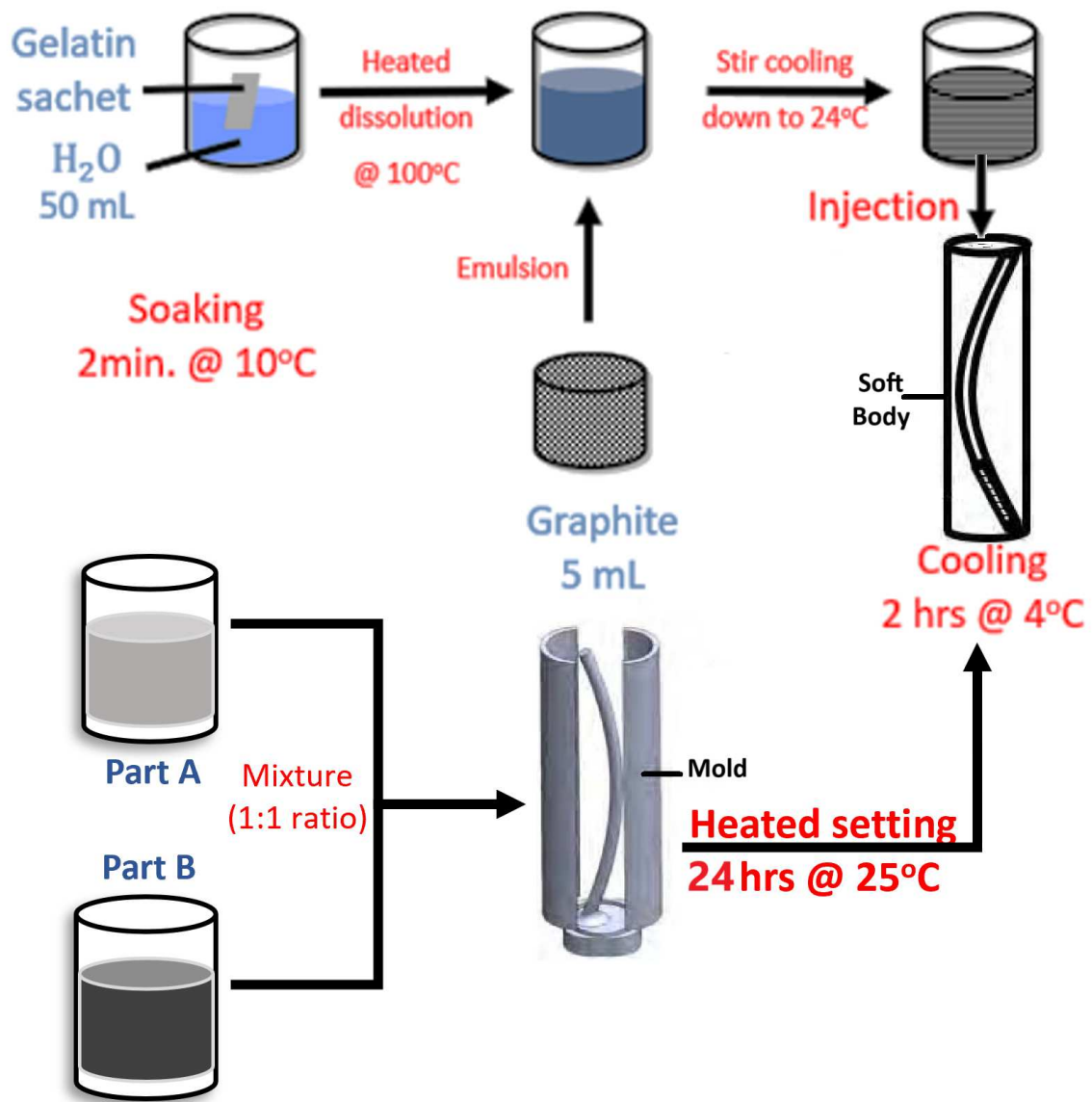


Figure 3.2: Fabrication process of the soft sensor.

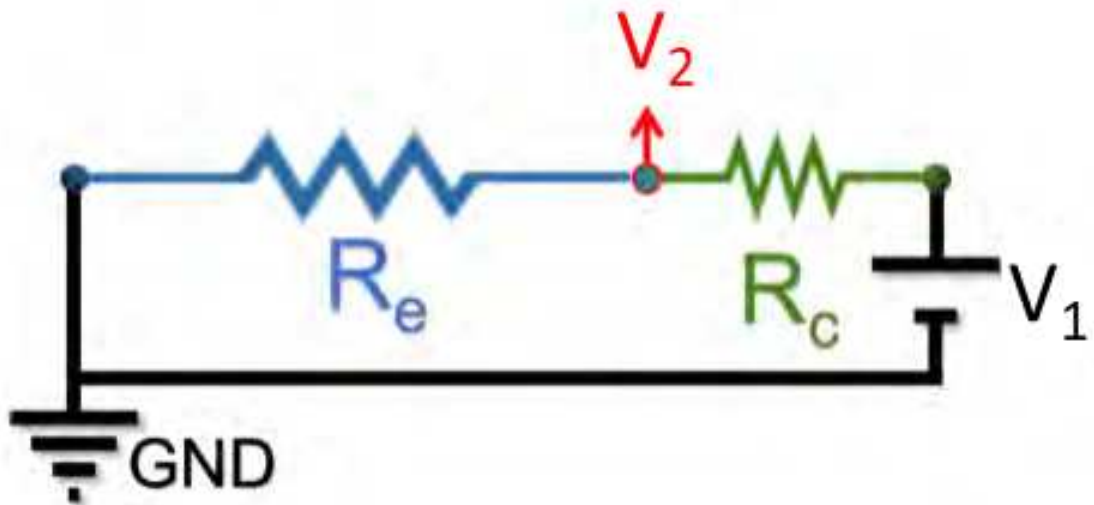
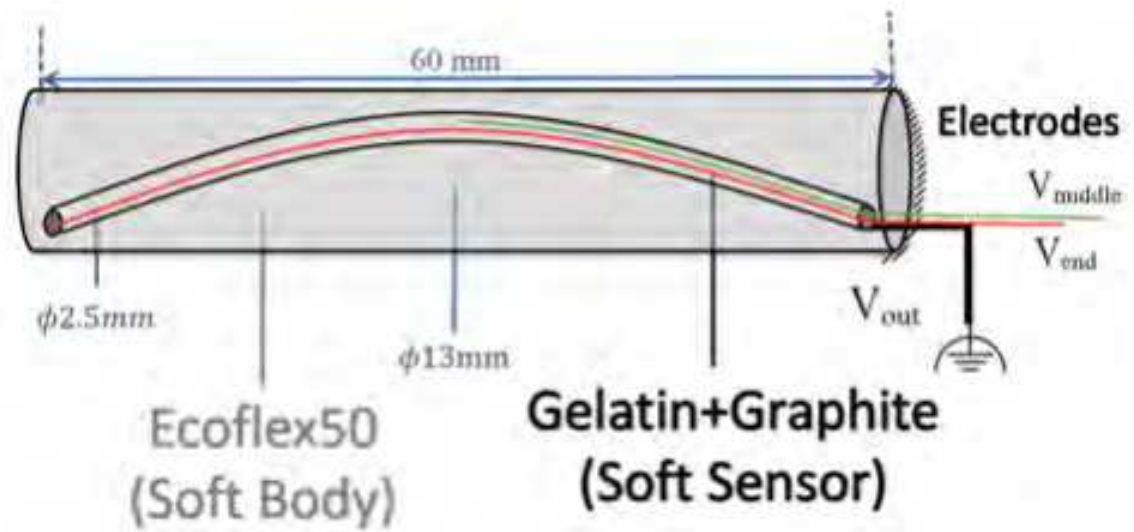


Figure 3.3: Top: the structural design of the sensor with a gelatin/graphite sensing element. The sensor tip is at the left end. Bottom: a simplified electrical model of the sensor and voltage splitter circuit.

Table 3.1: Composition and contents of the fabricated gelatin-based sensor

Sensing Element	Volume Fraction (%)		
	Water	Gelatin	Graphite
	70.1	14.1	15.8
Soft Body Components	Ecoflex 00-50 (Part A)	Ecoflex 00-50 (Part B)	
	50	50	

sensing material in place. Ecoflex 00-50 was combined in a 1 to 1 ratio, stirred for 5 minutes, and then allowed to degas under a vacuum of 101 kPa. After being injected into the molds, the mixture was allowed to settle for 24 hours at 25°C. The sensing component was fabricated by incorporating graphite micro platelets into the gelatin. The gelatin sachets were dissolved by stirring them after being immersed in cold water for two minutes. This emulsion was injected into the chamber of the soft body, after mixing it with graphite micro platelets, as is illustrated in Fig. 3.2. A summary of the materials and percentages of the composition of the fabricated sensing composite is presented in Table 3.1.

### 3.2.2 Experimental Setup and Data Acquisition

Fig. 3.4 depicts the fabricated flexural robot with the embedded sensing element and the experimental validated setup used in this study [34], consisting of a Gamma force and torque sensor (ATI Industrial Automation, NC, USA) to measure the ground truth force values acting on the flexural robot and sensing element. In a single trial of the experiment, arbitrary forces were applied to the tip of the sensor in all directions ( $X$ ,  $Y$  and  $Z$ ), and they were complex in nature, potentially comprising normal, shear, and other force components. An Arduino Uno was used to measure  $V_1$  and  $V_2$  raw data at a 250 Hz refresh rate and transfer the data to a PC. A user interface software for data acquisition, curation, storage, and post-processing was developed in C# programming language, integrating the software on the PC, the firmware on Arduino Uno, and the hardware (sensor and flexure). The data post-processing and calibration were performed in Matlab 2023a (Mathworks, MA, USA).

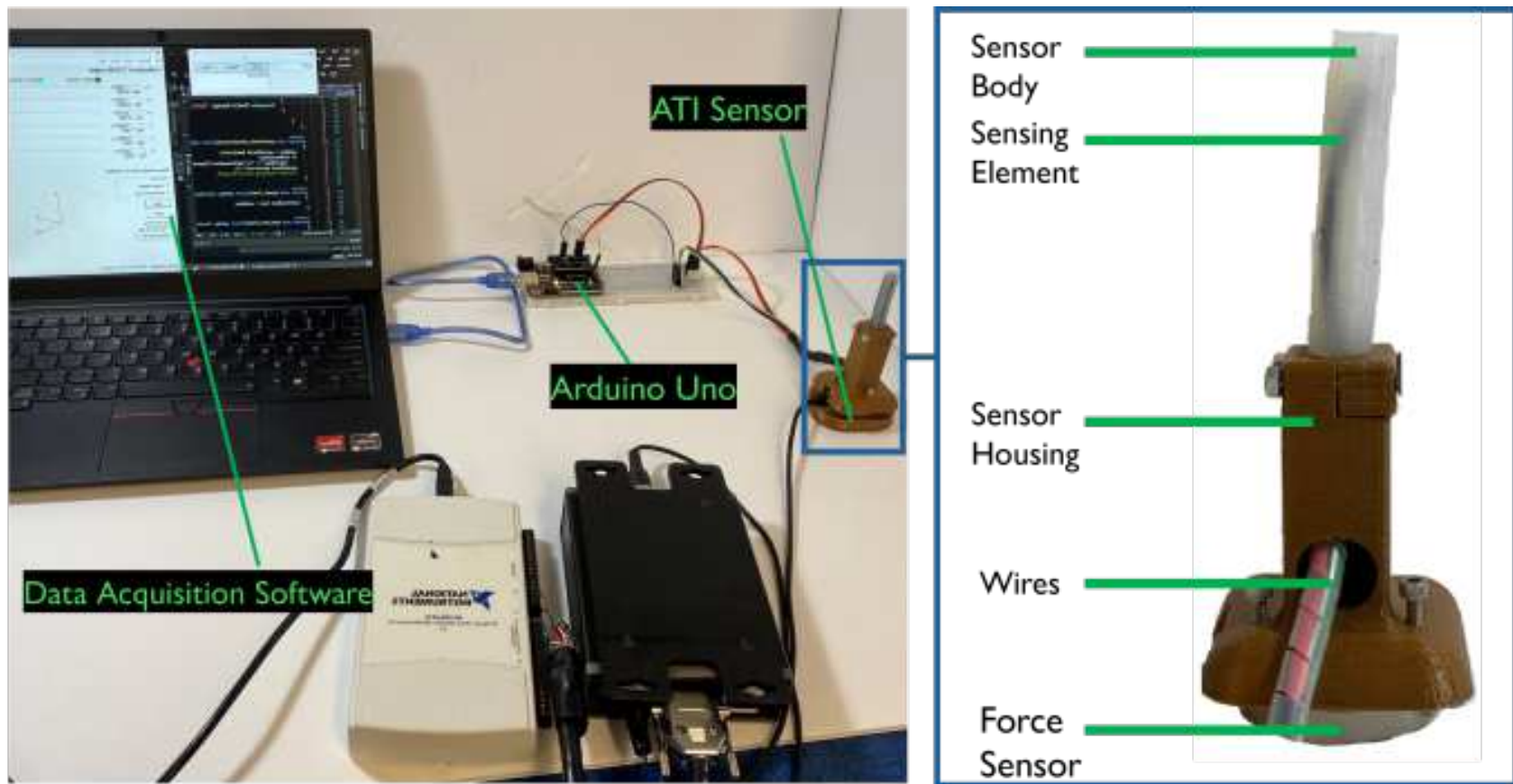


Figure 3.4: The fabricated sensor and flexural robot prototype, and the experimental setup used in data acquisition of this study.

### 3.2.3 Data Transformation

Data comprises two sets of voltage signals, namely  $z(t)$ , collected over time. In a previous work [1], such voltage signals were kept in the time domain and fed to a neural network, so no information containing frequency components was processed. However, the focus in this study is to enhance the calibration process by considering the features in the frequency domain while the temporal data is still being processed. Three types of transforms are implemented to extract such frequency components from the voltage signals in the form of time series. The first approach is based on three generalized wavelets: the morse wavelet, morlet wavelet, and bump wavelet [71]. The second method uses a real-time constant Q parameter where the center frequency to bandwidth ratio is constant, even though distinct time frames have variable center frequencies and bandwidths [61]. The third technique is a short-time Fourier transform (STFT) which represents a sort of trade-off between time and frequency-based views of a signal with limited accuracy, where the size of the frames determines that accuracy. These functions were studied to find the best candidates for input data that achieve the best regression results.

The STFT is based on the fundamental continuous form as defined in Eq. 4 [61, 72].

$$Z(\tau, w) = \int_{-\infty}^{\infty} z(t)w(t - \tau)e^{-iwt} dt \quad (4)$$

where  $z(t)$  denotes the original signal being investigated, and  $Z(\tau, w)$  represents the outcome of applying the STFT at a specific time window function of  $\tau$ . Wavelet families differ due to the numerous trade-offs each family provides regarding the wavelet's appearance, which can be both smooth and compact. This indicates that a wavelet family may be selected based on how much it matches the characteristics searched for in the data. Each wavelet type has a unique form, smoothness, and compactness, making it valuable for various applications [73]. Specifically, the three wavelet transform functions used in this work are the Morlet, Morse, and Bump. The continuous wavelet transform can help investigate the time-frequency-localized variability of a signal  $z(t)$  as described in Eq. 5.

$$Z(a, b) = \frac{1}{\sqrt{a}} \int_{-\infty}^{\infty} \overline{\psi\left(\frac{t-b}{a}\right)} z(t) dt \quad (5)$$

By changing the parameters  $a$  and  $b$ , the time and frequency variances of the output can be adjusted. For example, in the Morlet transform, time and frequency can be tuned to contribute equally to the output signal while, Morse wavelets can have a greater frequency variance, and for the Bump wavelets, the time variance can be larger. Here, It is demonstrated that how the generalized Morse wavelets combine all of the previously stated wavelet types into a single, wide-ranging family. These wavelets are defined in the frequency domain as

$$\Psi_{\beta,\gamma}(\omega) = \int_{-\infty}^{\infty} \psi_{\beta,\gamma}(t)e^{-i\omega t} dt = U(\omega)a_{\beta,\gamma}\omega^{\beta}e^{-\omega\gamma} \quad (6)$$

where  $a_{\beta,\gamma}$  is a normalization constant,  $U(\omega)$  is the unit step function, and  $\beta$  and  $\gamma$  are two parameters controlling the wavelet form [71],[74].

### 3.2.4 Transfer Learning Calibration

Same as the approach in the previous chapter, Fig. 3.5 shows an overview of the whole process of the proposed calibration method. Convolutional neural networks have been used to address the significantly high non-linearity and hysteresis of the soft sensor. This research investigates a calibration method based on deep learning, as an alternative and improved method that offers a derivative-free approach for calibration of the designed soft embedded sensor.

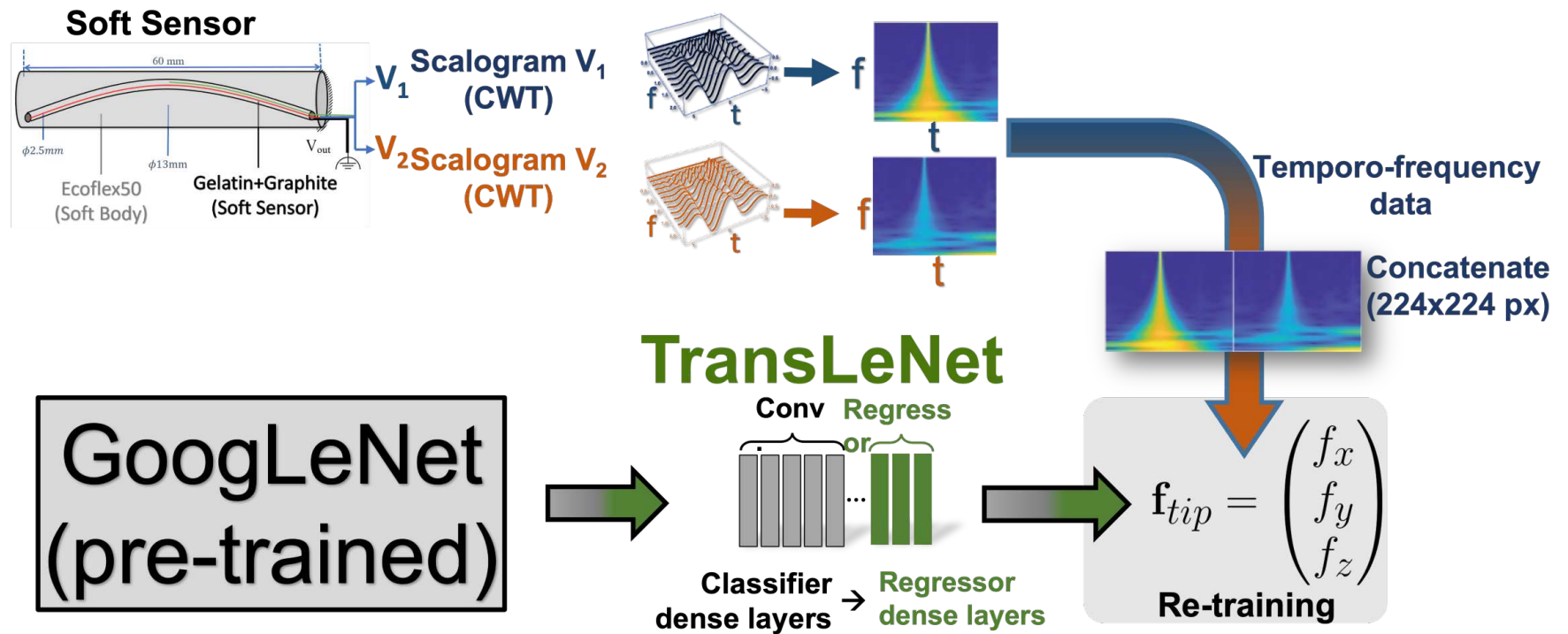


Figure 3.5: Dataflow-gram of the proposed transfer-learning-based calibration method.

A previously trained neural network from GoogLeNet (Alphabet Inc.) was utilized, due to the small size of the data set, consisting of 22 layers (including convolutional and max pooling). For input features of the proposed neural model, vectors  $X$  and  $Y$  were selected as

$$X = \begin{pmatrix} V_1 & V_2 \\ \widehat{V}_1 & \widehat{V}_2 \end{pmatrix}^T \quad (7)$$

$$Y = (F_x \quad F_y \quad F_z)^T \quad (8)$$

The input layer of the neural network had two neurons to receive the voltage signals  $V_1$  and  $V_2$ , and the initial voltages  $\widehat{V}_1$  and  $\widehat{V}_2$  measured with no excitation applied to the sensor. The output layer had three neurons dedicated to generating the estimated forces  $F$  in the x, y, and z directions. The torques were not considered in this work to simplify the network implementation but will be considered in future experiments. The last layer of the GoogLeNet (classifier) was replaced with eight fully connected layers of 750, 500, 250, 150, 100, 50, 10, and 3 neurons with a rectified linear unit (ReLU) activation function to perform the force estimation (regression). This architecture was chosen empirically based on observation of the performance. In the future works, a complete hyper-parameter search must be done for optimized architectural design. Beyond this point, the reconstructed convolutional calibration model is referred as `TransLeNet`. The force signals were normalized for improved precision during training, and the 'adam' optimizer was used with 20 iterations. For training, validation, and test allocation, the training data set was divided with a split ratio of 70:15:15, using the Matlab Deep Learning Tool Box (Mathworks, MA, USA).

### 3.2.5 Training Dataset

Scalograms were obtained for the Continuous Wavelet Transform (CWT), Constant Q Transform (CQT), and Short Time Fourier Transform (STFT) of the two voltages  $V_1$  and  $V_2$  recorded during sensor calibration. Scalograms were 2D pictures in the RGB color-space, as illustrated in Fig. 3.5 and 3.7. To be more precise, the CWTs were generated using the Morse, Bump, and Morlet (Gabor) wavelets with a predetermined Gamma value ( $\gamma$ ). The input picture for the transferred neural network was created by horizontally concatenating the  $224 \times 112$  px CWT images in the form

of  $[V_1 V_2]$  with the final resolution of  $224 \times 224$ . In addition, a Synchrosqueezing technique was added to the wavelet to enhance the scalogram's temporal resolution. Synchrosqueezing is a helpful method for time-frequency analysis of signals with oscillating components, such as physiological signals and machine vibrations [75, 76, 77]. The calibration process provided a total of 70 pairs of scalograms.

### **3.2.6 Validation Protocol**

In a previous study, forces were predicted by transferring the calibration model to the developed user interface. Concurrently, the ground-truth force measurements of the ATI sensor were acquired. Similar to training evaluation, the soft body was manually deformed at its tip throughout the test. Following that, the inaccuracy was analyzed by comparing the anticipated forces with the actual values. The time variations in the predicted and ground-truth forces in the validation experiment are reported in the results section.

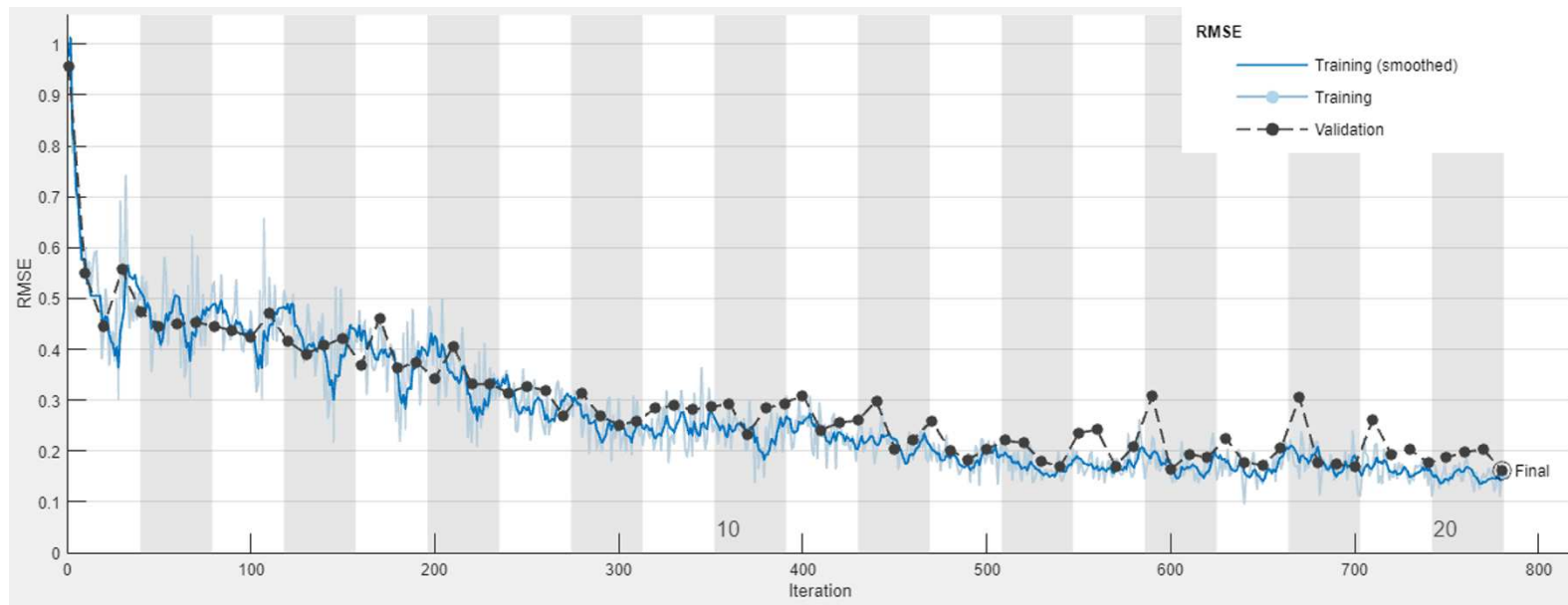


Figure 3.6: Progress of training the proposed calibration method with the training dataset. The RMSE constantly decreased until no further improvement was possible through gradient decent on TransLeNet.

### 3.3 Results and Discussion

#### 3.3.1 Calibration Verification

The goodness of fit ( $R^2$ ) and Root Mean Squared Error (RMSE) metrics were used to assess TransLeNet's performance, after 20 epochs and 800 iterations, as shown in Fig. 3.6. The  $R^2$  score of the representative transform (Morse) for  $F_x$ ,  $F_y$ , and  $F_z$  was determined to be 95%, 97%, and 97.3%, respectively, which proves that it is a remarkable fit for the model and target variable. The RMSE, which measures the average squared difference between the predicted and actual values, was 0.295 mN. This means the model has a relatively low error and well predicts the target variable.

#### 3.3.2 Experimental Validation

A performance comparison of the five suggested transforms is shown in Fig. 3.7. To this end, the suggested calibration method for unseen data from tip force prediction in the X direction is illustrated, i.e.  $F_x$ . For each transform, the Mean Absolute Error (MAE) and Maximum Absolute Error (MaxAE) of the predicted force were obtained based on the ground truth (reference). Error metrics are shown in Table 3.2.

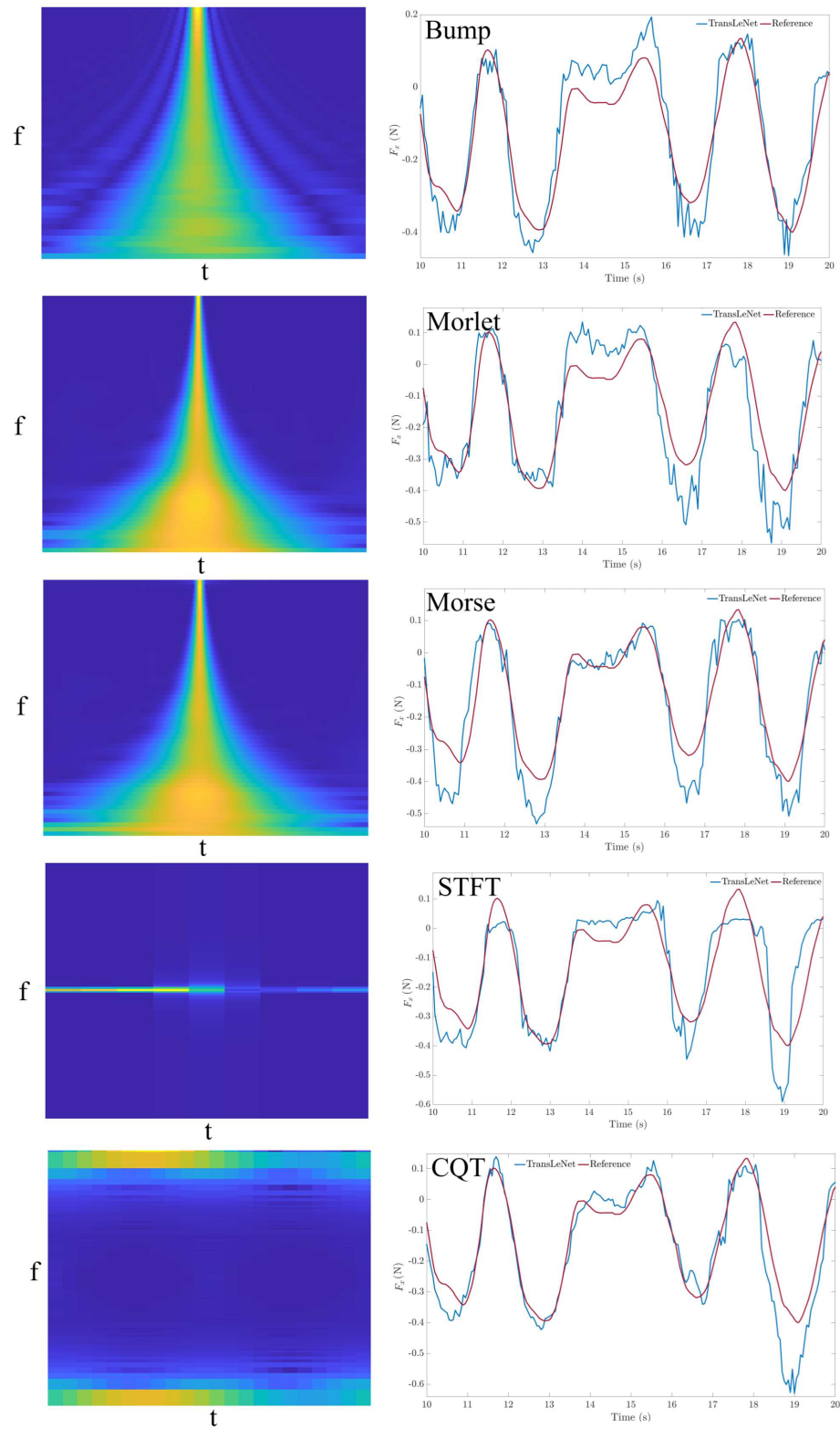


Figure 3.7: Sample scalograms as inputs to TransLeNet and output forces for all transformations. Forces are compared between estimations and references.

To illustrate the best calibration results, Fig. 3.8 shows the reference and estimated forces using the Morse transform. Correlation graphs are included to visually perceive the similarity between the estimated forces from the calibration model and the ground truth. The Morse transform is the best calibration model as it had a strong correlation with an  $R^2$  value greater or equal to 0.95 for all axes of force. This also indicates that the proposed calibration model was successful in predicting the correct forces despite large deformation, nonlinearity effects, and noise in the voltage measurement. It was also qualitatively observed that the error was not amplified at near zero forces in contrast to the recent finding in [1] that suggested otherwise. The reason for this is that the new method includes derivative-free data, whereas, in the previous study, a derivative-based calibration was used. Therefore, noise amplification was inevitable, especially in near zero forces where the energy of the noise in the signal becomes comparable to the total signal's energy. To portray the proposed calibration within the context of the current literature, a comparison with a series of representative studies is summarized in Table 3.3. The major finding of the comparison was that the sensor showed

Table 3.2: Performance metrics based on transformations and degrees of freedom

<b>Transformation</b>	<b>DOF</b>	<b>Error Ranges (mN)</b>	<b>MAE* (mN)</b>	<b>MaxAE** (mN)</b>
Morse	$F_x$	-160 , 190	4.7	194
	$F_y$	-90 , 190	4.5	194
	$F_z$	-70 , 290	7.9	286
Morlet	$F_x$	-190 , 310	7.3	307
	$F_y$	-520 , 180	11.4	515
	$F_z$	-80 , 470	16.8	467
Bump	$F_x$	-180 , 220	5.6	217
	$F_y$	-170 , 260	5.2	259
	$F_z$	-120 , 360	8.3	357
CQT	$F_x$	-180 , 260	4.3	257
	$F_y$	-140 , 120	2.7	142
	$F_z$	-80 , 380	11.2	378
STFT	$F_x$	-390 , 210	6.7	395
	$F_y$	-350 , 280	5.9	350
	$F_z$	-150 , 650	24	651

\* **MAE:** Mean Absolute Error

\*\* **MaxAE:** Maximum Absolute Error

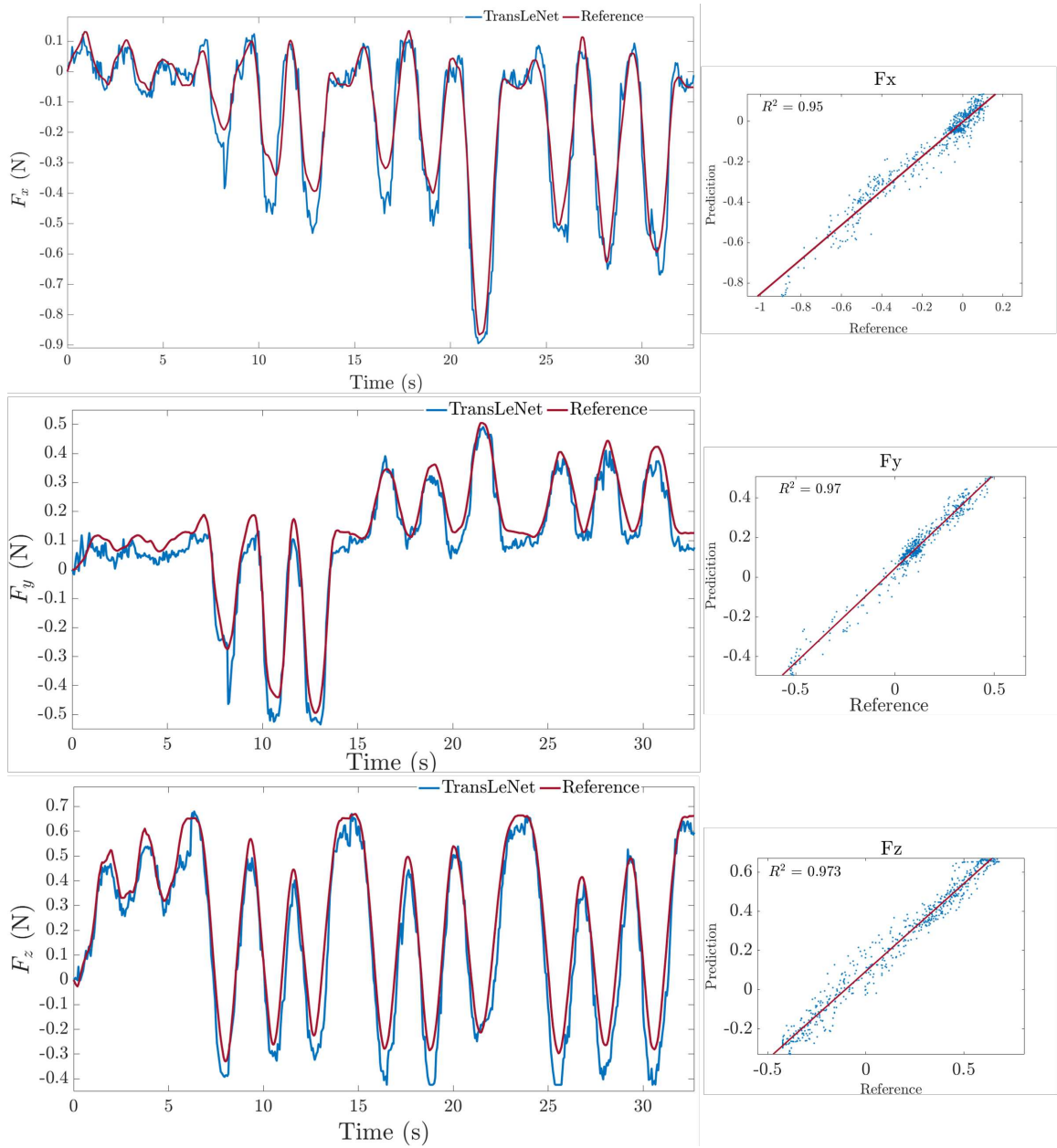


Figure 3.8: Comparison of reference forces and estimated forces with Morse transform. The graphs on the right show the corresponding correlations.

Table 3.3: Calibration performance compared to other representative studies

Study	Sensing principle	Calibration	Min. Detectable	Range
Rehan <i>et al.</i> [78] (2022)	Magnetic	Hall effect	250 mN	0 - 20 N
Yang <i>et al.</i> [79] (2022)	Magnetic	-	50 mN	0 - 4 N
Massari <i>et al.</i> [80] (2022)	FBG	DNN	35 mN	0-2.5 N
Bandari <i>et al.</i> [36] (2020)	LIM	SVM	50 mN	0-2 N
Atoche <i>et al.</i> [81] (2022)	PR	SPI	39 mN	0.392 - 4.905 N
Torkaman <i>et al.</i> [1] (2023)	PR	MLP	$\leq 1$ mN	0 - 0.350 N
Masoumi <i>et al.</i> [50] (2023)	PR	WaveLeNet	$\leq 1$ mN	0 - 0.397 N
Masoumi <i>et al.</i> [52] (2024)	PR	TransLeNet	$\leq 1$ mN	0 - 0.397 N

<b>FBG:</b> Fiber-Bragg Grating	<b>DNN:</b> Deep Neural Network
<b>LIM:</b> Light Intensity Modulation	<b>SVM:</b> Support Vector Regression
<b>PR:</b> Piezoresistive	<b>SPI:</b> Serial Peripheral Interface
	<b>MLP:</b> Multi-Layer Perceptron

a relatively more limited range while exhibiting a smaller minimum detectable force. This implies that the proposed sensor has a smaller resolution ( $\leq 1\text{mN}$ ). Another finding of the comparison was that the proposed calibration schema was the only one that used a convolutional deep-learning approach. A major contribution of this work was in fusing multiple signals into one image (through transformation) and using that within a deep-learning model for inference (regression modelling). The fact that a transfer learning approach is used, saved time in developing feature extraction layers; whereas without transfer learning one would need to build the entire network from scratch which might result in suboptimal accuracy due to the need for a high volume of images and training data.

The results show that using the Morse transform, the proposed calibration method resulted in comparable accuracy and minimum detectable force to the previously proposed calibration model with derivative-based features [1]. However, compared to the previous results [1], this study indicates that the proposed calibration with Morse transform provides less noise in force estimation and more accuracy for forces below 100 mN of amplitude. Moreover, the combined sensor and calibration method showed a lower range of measurement than those of other authors, perhaps due to a combination of a highly compliant flexure (supporting substrate) and the configuration of the sensing element, which is directly affected by the flexure material. This observation applies to previous findings as well [1].

### 3.4 Summary

In this chapter, the design and fabrication process of the soft sensor is described. Additionally, five transformations, including CQT and STFT discussed in the previous chapter, are examined and compared. The best transformation is selected for the application in question, based on various metrics like linearity ( $R^2$ -score), mean absolute error (MAE), and maximum absolute error (MaxAE). An enhanced and expanded calibration framework, 'TransLeNet', is introduced, evaluating five time-frequency signal transformations—Morse, Morlet, Bump, Constant Q (CQT), and Short-Time Fourier Transform (STFT). This comparison highlights their effectiveness in resolution and sensing range with the soft sensor, and identifies the best performing model.

## Chapter 4

# Conclusions and Future Works

### 4.1 Conclusions

Embedded piezoresistive force sensors for soft robots can be fabricated with gelatin and graphite materials as sensing elements. A precise calibration procedure is required to compensate for the nonlinear behaviours of soft sensors. In noisy surroundings, the sensor's accuracy is drastically affected, and rate-dependent characteristics applied in the neural calibration amplify electromagnetic interference and noise. To address these challenges, a novel calibration technique was introduced that utilizes 2D time-frequency signal representations instead of traditional 1D signals (data). By transforming these signals into two-dimensional scalograms, capturing a richer array of image features was more feasible. Two signals of voltages were concatenated into one image (through transformation). These signals were used within a deep-learning model for inference (regression modelling), saving time in developing feature extraction layers and avoiding the need for a high volume of images and training data. The proposed calibration technique based on morse transform is derivative-free and included temporal variations of electrical signals from soft sensors by capturing image features in various transform scalograms. In comparison to the previously verified rate-dependent calibration, TransLeNet provided high accuracy and minimum detectable force throughout the whole range of our soft flexural sensor, comparable to the previous derivative-based method [1], except with less noise in force estimation and more accuracy for forces up to 100 mN of amplitude.

## 4.2 Future Works

To build upon the current research and improve the sensor's performance in MIS procedures, future studies could focus on the following areas:

- (1) Extending the range of the force sensing to meet the requirements of MIS procedures better by optimizing the sensor material properties and structural design.
- (2) Design improvements and geometric modifications of the sensing element to integrate novel microfabrication techniques that could allow for more precise force measurements within the required range.
- (3) Advanced calibration techniques to be performed in real-time for the enhancement of the final outcome.
- (4) Integration into surgical robotics models available and evaluating the performance of the sensor in a controlled environment, simulating real MIS scenarios.

# Bibliography

- [1] Tannaz Torkaman, Majid Roshanfar, Javad Dargahi, and Amir Hooshidar. Embedded six-dof force-torque sensor for soft robots with learning-based calibration. *IEEE Sensors Journal*, in-press:1–1, 2023.
- [2] Amir Hooshidar, Siamak Najarian, and Javad Dargahi. Haptic telerobotic cardiovascular intervention: a review of approaches, methods, and future perspectives. *IEEE reviews in biomedical engineering*, 13:32–50, 2019.
- [3] Naghmeh Bandari, Javad Dargahi, and Muthukumaran Packirisamy. Tactile sensors for minimally invasive surgery: A review of the state-of-the-art, applications, and perspectives. *Ieee Access*, 8:7682–7708, 2019.
- [4] Allison M Okamura. Haptic feedback in robot-assisted minimally invasive surgery. *Current opinion in urology*, 19(1):102, 2009.
- [5] Olatunji Mumini Omisore, Shipeng Han, Jing Xiong, Hui Li, Zheng Li, and Lei Wang. A review on flexible robotic systems for minimally invasive surgery. *IEEE Transactions on Systems, Man, and Cybernetics: Systems*, 52(1):631–644, 2022.
- [6] I. Sahin and B. Baca. Robotic-assisted laparoscopic complete mesocolic excision. *Digestive Disease Interventions*, 07:024–029, 2023. doi: 10.1055/s-0042-1760369.
- [7] J. Kim, M. d. Mathelin, K. Ikuta, and D. Kwon. Advancement of flexible robot technologies for endoluminal surgeries. *Proceedings of the IEEE*, 110:909–931, 2022. doi: 10.1109/jproc.2022.3170109.

- [8] Z. Yang, H. Yang, Y. Cao, Y. Cui, and Z. Zhang. Magnetically actuated continuum medical robots: a review. *Advanced Intelligent Systems*, 5, 2023. doi: 10.1002/aisy.202200416.
- [9] M. Miyasaka, J. Liu, L. Cao, W. Lai, X. Li, A. M. H. Tiong, C. L. Lim, B. W. J. Quek, H. L. Kaan, D. Dolgunov, K. Y. Ho, and S. J. Phee. Flexible and deployable colon support structure for endoluminal interventions. *IEEE Access*, 9:91754–91763, 2021. doi: 10.1109/access.2021.3090411.
- [10] S. Abeywardena, Q. Yuan, A. Tzemanaki, E. Psomopoulou, L. Droukas, M. Chris, and S. Dogramadzi. Estimation of tool-tissue forces in robot-assisted minimally invasive surgery using neural networks. *Frontiers in Robotics and AI*, 6, 2019. doi: 10.3389/frobt.2019.00056.
- [11] L. Yu, Y. Yan, C. Li, and X. Zhang. Three-dimensional nonlinear force-sensing method based on double microgrippers with e-type vertical elastomer for minimally invasive robotic surgery. *Robotica*, 36:865–881, 2018. doi: 10.1017/s0263574718000085.
- [12] S. Wang, Z. Liu, X. Shu, and L. Xie. Mechanism design and force sensing of a novel cardiovascular interventional surgery robot. *The International Journal of Medical Robotics and Computer Assisted Surgery*, 18, 2022. doi: 10.1002/rcs.2406.
- [13] Ali Mehrjouyan, Mohammad B Menhaj, and Amir Hooshier. Safety-enhanced observer-based adaptive fuzzy synchronization control framework for teleoperation systems. *European Journal of Control*, 73:100885, 2023.
- [14] Ali Mehrjouyan, Mohammad B Menhaj, and Amir Hooshier. Adaptive-neural command filtered synchronization control of tele-robotic systems using disturbance observer with safety enhancement. *Journal of the Franklin Institute*, 361(13):107036, 2024.
- [15] Matteo Cianchetti, Cecilia Laschi, Arianna Menciassi, and Paolo Dario. Biomedical applications of soft robotics. *Nature Reviews Materials*, 3(6):143–153, 2018.
- [16] K. Li, B. Pan, F. Zhang, W. Gao, Y. Fu, and S. Wang. A novel 4-dof surgical instrument with modular joints and 6-axis force sensing capability. *The International Journal of Medical Robotics and Computer Assisted Surgery*, 13:e1751, 2016. doi: 10.1002/rcs.1751.

- [17] S. Rodrigues, T. Horeman, P. Sam, J. Dankelman, J. Dobbela, and F. Jansen. Influence of visual force feedback on tissue handling in minimally invasive surgery. *British Journal of Surgery*, 101:1766–1773, 2014. doi: 10.1002/bjs.9669.
- [18] H. Shi, B. Zhang, X. Mei, and Q. Song. Realization of force detection and feedback control for slave manipulator of master/slave surgical robot. *Sensors*, 21:7489, 2021. doi: 10.3390/s21227489.
- [19] Amir Hooshidar, Masoud Razban, Naghmeh M Bandari, and Javad Dargahi. Sensing principle for real-time characterization of viscoelasticity in the beating myocardial tissue. In *2017 IEEE International Conference on Computational Intelligence and Virtual Environments for Measurement Systems and Applications (CIVEMSA)*, pages 72–77. IEEE, 2017.
- [20] Amir Hooshidar, NM Bandari, Bandari, and Javad Dargahi. Image-based estimation of contact forces on catheters for robot-assisted cardiovascular intervention. In *The Hamlyn Symposium on Medical Robotics*, volume 1, pages 119–120, 2018.
- [21] Mohammad Jolaei, Amir Hooshidar, Amir Sayadi, Javad Dargahi, and Muthukumar Packirisamy. Sensor-free force control of tendon-driven ablation catheters through position control and contact modeling. In *2020 42nd annual international conference of the IEEE engineering in medicine and biology society (EMBC)*, pages 5248–5251. IEEE, 2020.
- [22] Mohammad Jolaei, Amir Hooshidar, Javad Dargahi, and Muthukumar Packirisamy. Toward task autonomy in robotic cardiac ablation: Learning-based kinematic control of soft tendon-driven catheters. *Soft Robotics*, 8(3):340–351, 2021.
- [23] Pegah Yaftian, Naghmeh Bandari, Amir Hooshidar, and Javad Dargahi. Image-based contact detection and static force estimation on steerable rfa catheters. In *2020 International Conference on Biomedical Innovations and Applications (BIA)*, pages 57–60. IEEE, 2020.
- [24] Amir Hooshidar, Amir Sayadi, Mohammad Jolaei, and Javad Dargahi. Analytical tip force estimation on tendon-driven catheters through inverse solution of cosserat rod model. In *2021 IEEE/RSJ International Conference on Intelligent Robots and Systems (IROS)*, pages 1829–1834. IEEE, 2021.

- [25] Amir Sayadi, Hamid Reza Nourani, Mohammad Jolaei, Javad Dargahi, and Amir Hooshier. Force estimation on steerable catheters through learning-from-simulation with ex-vivo validation. In *2021 International Symposium on Medical Robotics (ISMR)*, pages 1–6. IEEE, 2021.
- [26] P. A. Ersman, J. Eriksson, D. Jakonis, S. Pantzare, J. Åhlin, J. Strandberg, S. Sundin, H. Toss, F. Ahrentorp, K. Daoud, C. Jonasson, H. Svensson, G. Gregard, U. Näslund, and C. Johansson. Integration of screen printed piezoelectric sensors for force impact sensing in smart multifunctional glass applications. *Advanced Engineering Materials*, 24, 2022. doi: 10.1002/adem.202200399.
- [27] C. Zhe, J. S. Du, and Y. Y. Liu. Research on pvdf micro-force sensor. *Applied Mechanics and Materials*, 599-601:1135–1138, 2014. doi: 10.4028/www.scientific.net/amm.599-601.1135.
- [28] Maria Antonia Cassa, Martina Maselli, Alice Zoso, Valeria Chiono, Letizia Fracchia, Chiara Ceresa, Gianluca Ciardelli, Matteo Cianchetti, and Irene Carmagnola. Development of an innovative soft piezoresistive biomaterial based on the interconnection of elastomeric pdms networks and electrically-conductive pedot: Pss sponges. *Journal of Functional Biomaterials*, 13(3):135, 2022.
- [29] S. J. Park, J. C. Doll, A. Rastegar, and B. L. Pruitt. Piezoresistive cantilever performance—part ii: optimization. *Journal of Microelectromechanical Systems*, 19:149–161, 2010. doi: 10.1109/jmems.2009.2036582.
- [30] B. Komati, J. Agnus, C. Clevey, and P. Lutz. Prototyping of a highly performant and integrated piezoresistive force sensor for microscale applications. *Journal of Micromechanics and Microengineering*, 24:035018, 2014. doi: 10.1088/0960-1317/24/3/035018.
- [31] M. Pacheco, F. M. Santoyo, A. Méndez, and L. Zenteno. Piezoelectric-modulated optical fibre bragg grating high-voltage sensor. *Measurement Science and Technology*, 10:777–782, 1999. doi: 10.1088/0957-0233/10/9/303.
- [32] B. Li, B. G. Rosa, M. Power, A. Gao, S. Treratanakulchai, S. Anastasova, and G. Yang. Carbon-nanotube-coated 3d microspring force sensor for medical applications. *ACS Applied Materials and Amp; Interfaces*, 11:35577–35586, 2019. doi: 10.1021/acsami.9b12237.

- [33] Naghmeh M Bandari, Roozbeh Ahmadi, Amir Hooshier, Javad Dargahi, and Muthukumaran Packirisamy. Hybrid piezoresistive-optical tactile sensor for simultaneous measurement of tissue stiffness and detection of tissue discontinuity in robot-assisted minimally invasive surgery. *Journal of biomedical optics*, 22(7):077002–077002, 2017.
- [34] Tannaz Torkaman, Majid Roshanfar, Javad Dargahi, and Amir Hooshier. Accurate embedded force sensor for soft robots with rate-dependent deep neural calibration. In *2022 IEEE International Symposium on Robotic and Sensors Environments (ROSE)*, pages 1–7. IEEE, 2022.
- [35] Torkaman Tannaz, Majid Roshanfar, Javad Dargahi, and Amir Hooshier. Analytical modeling and experimental validation of a gelatin-based shape sensor for soft robots. In *2022 International Symposium on Medical Robotics (ISMR)*, pages 1–7. IEEE, 2022.
- [36] Naghmeh Bandari, Javad Dargahi, and Muthukumaran Packirisamy. Image-based optical-fiber force sensor for minimally invasive surgery with ex-vivo validation. *Journal of The Electrochemical Society*, 167(12):127504, 2020.
- [37] Vinod Nair and Geoffrey E Hinton. Rectified linear units improve restricted boltzmann machines. In *Proceedings of the 27th international conference on machine learning (ICML-10)*, pages 807–814, 2010.
- [38] Luxian Wang, Huiling Peng, Xiaolin Wang, Xiang Chen, Chunsheng Yang, Bin Yang, and Jingquan Liu. Pdms/mwcnt-based tactile sensor array with coplanar electrodes for crosstalk suppression. *Microsystems and nanoengineering*, 2(1):1–8, 2016.
- [39] Yanan Ma, Nishuang Liu, Luying Li, Xiaokang Hu, Zhengguang Zou, Jianbo Wang, Shijun Luo, and Yihua Gao. A highly flexible and sensitive piezoresistive sensor based on mxene with greatly changed interlayer distances. *Nature communications*, 8(1):1207, 2017.
- [40] Minxuan Xu, Feng Li, Zhenyun Zhang, Tao Shen, Qian Zhang, and Junjie Qi. Stretchable and multifunctional strain sensors based on 3d graphene foams for active and adaptive tactile imaging. *Science China Materials*, 62(4):555–565, 2018.

- [41] Hu Liu, Mengyao Dong, Wenju Huang, Jiachen Gao, Kun Dai, Jiang Guo, Guoqiang Zheng, Chuntai Liu, Changyu Shen, and Zhanhu Guo. Lightweight conductive graphene/thermoplastic polyurethane foams with ultrahigh compressibility for piezoresistive sensing. *Journal of Materials Chemistry C*, 5(1):73–83, 2017.
- [42] Jin Jia, Guotao Huang, Jianping Deng, and Kai Pan. Skin-inspired flexible and high-sensitivity pressure sensors based on rgo films with continuous-gradient wrinkles. *Nanoscale*, 11(10):4258–4266, 2019.
- [43] János Radó, Csaba Dücső, Péter Földesy, Gábor Szebényi, Zbigniew Nawrat, Kamil Rohr, and Péter Fürjes. 3d force sensors for laparoscopic surgery tool. *Microsystem Technologies*, 24:519–525, 2018.
- [44] Tingting Zhao, Tongkuai Li, Longlong Chen, Li Yuan, Xifeng Li, and Jianhua Zhang. Highly sensitive flexible piezoresistive pressure sensor developed using biomimetically textured porous materials. *ACS applied materials and interfaces*, 11(32):29466–29473, 2019.
- [45] Chanhyuk Lim, Yoonsoo Shin, Jaebong Jung, Ji Hoon Kim, Sangkyu Lee, and Dae-Hyeong Kim. Stretchable conductive nanocomposite based on alginate hydrogel and silver nanowires for wearable electronics. *APL Materials*, 7(3):031502, 2019.
- [46] Markus Hessinger, Tobias Pilic, Roland Werthschützky, and Peter P Pott. Miniaturized force/torque sensor for in vivo measurements of tissue characteristics. In *2016 38th Annual International Conference of the IEEE Engineering in Medicine and Biology Society (EMBC)*, pages 2022–2025. IEEE, 2016.
- [47] DongWook Kim and Yong-Lae Park. Contact localization and force estimation of soft tactile sensors using artificial intelligence. In *2018 IEEE/RSJ International Conference on Intelligent Robots and Systems (IROS)*, pages 7480–7485. IEEE, 2018.
- [48] DongWook Kim, Junghan Kwon, Byungjun Jeon, and Yong-Lae Park. Adaptive calibration of soft sensors using optimal transportation transfer learning for mass production and long-term usage. *Advanced Intelligent Systems*, 2(6):1900178, 2020.

- [49] Seunghyun Han, Taekyoung Kim, Dooyoung Kim, Yong-Lae Park, and Sungho Jo. Use of deep learning for characterization of microfluidic soft sensors. *IEEE Robotics and Automation Letters*, 3(2):873–880, 2018.
- [50] Navid Masoumi, Negar Kazemipour, Sarvin Ghiasi, Tannaz Torkaman, Amir Sayadi, Javad Dargahi, and Amir Hooshier. Wavelenet: Transfer neural calibration for embedded sensing in soft robots. In *Hamlyn Symposium on Medical Robotics*, 2023.
- [51] Navid Masoumi, Andrés C. Ramos, Tannaz Torkaman, Liane S. Feldman, Jake Barralet, Javad Dargahi, and Amir Hooshier. Embedded force sensor for soft robots with deep transformation calibration. *IEEE Transactions on Medical Robotics and Bionics*, 6(4):1363–1374, 2024. doi: 10.1109/TMRB.2024.3479878.
- [52] Navid Masoumi, Andres C Ramos, Tannaz Torkaman, Javad Dargahi, Jake Barralet, Liane S Feldman, and Amir Hooshier. Embedded force sensor with deep transformation calibration for interventional soft robots. In *2024 46th Annual International Conference of the IEEE Engineering in Medicine and Biology Society (EMBC)*, pages 1–4. IEEE, 2024.
- [53] Majid Roshanfar, Salar Taki, Amir Sayadi, Renzo Cecere, Javad Dargahi, and Amir Hooshier. Hyperelastic modeling and validation of hybrid-actuated soft robot with pressure-stiffening. *Micromachines*, 14(5):900, 2023.
- [54] B. Kim, S. Kong, and S. Kim. Low computational enhancement of stft-based parameter estimation. *IEEE Journal of Selected Topics in Signal Processing*, 9:1610–1619, 2015. doi: 10.1109/jstsp.2015.2465310.
- [55] F. Xie, W. Gan, J. Shang, H. Liu, Q. Xiao, and X. San-mao. Gearbox fault diagnosis method based on multidomain information fusion. *Sensors*, 23:4921, 2023. doi: 10.3390/s23104921.
- [56] L. Li, H. Cai, H. Han, Q. Jiang, and H. Ji. Adaptive short-time fourier transform and synchrosqueezing transform for non-stationary signal separation. *Signal Processing*, 166:107231, 2020. doi: 10.1016/j.sigpro.2019.07.024.

- [57] Jae Myung Kim, Gyuhoo Choi, and Sungbum Pan. User identification system based on 2d cqt spectrogram of emg with adaptive frequency resolution adjustment. *Scientific Reports*, 14(1): 1340, 2024.
- [58] J. Yang, P. Lin, and Q. He. Constant-q magnitude–phase coefficients extraction for synthetic speech detection. *IET Biometrics*, 9:216–221, 2020. doi: 10.1049/iet-bmt.2018.5100.
- [59] T. Sang, C. Zhao, Y. Wang, X. Gao, and L. Wang. Vibration transmission characteristic analysis of the metro turnout area by constant-q nonstationary gabor transform. *Measurement and Control*, 53:1739–1750, 2020. doi: 10.1177/0020294020952466.
- [60] D. S. D. V. L. N and K. S. R. Murty. Speech source separation using ica in constant q transform domain. *Interspeech 2018*, 2018. doi: 10.21437/interspeech.2018-1732.
- [61] Nicki Holighaus, Monika Dörfler, Gino Angelo Velasco, and Thomas Grill. A framework for invertible, real-time constant-q transforms. *IEEE Transactions on Audio, Speech, and Language Processing*, 21(4):775–785, 2012.
- [62] Pramod B Bachhav, Massimiliano Todisco, Moctar Mossi, Christophe Beaugeant, and Nicholas Evans. Artificial bandwidth extension using the constant q transform. In *2017 IEEE International Conference on Acoustics, Speech and Signal Processing (ICASSP)*, pages 5550–5554. IEEE, 2017.
- [63] Z. P. Zhang, A. Petit, J. Dequidt, and C. Duriez. Calibration and external force sensing for soft robots using an rgb-d camera. *IEEE Robotics and Automation Letters*, 4:2356–2363, 2019. doi: 10.1109/lra.2019.2903356.
- [64] W. Wei-dong, L. Zhang, and J. Ma. Kinematic calibration of 6-ups surgical parallel robot. *2013 ICME International Conference on Complex Medical Engineering*, pages 369–374, 2013. doi: 10.1109/iccme.2013.6548271.
- [65] D. Kim, S. Kim, T. Kim, B. B. Kang, M. Lee, W. Park, S. Ku, D. Kim, J. Kwon, H. Lee, J. Bae, Y. Park, K. Cho, and S. Jo. Review of machine learning methods in soft robotics. *Plos One*, 16:e0246102, 2021. doi: 10.1371/journal.pone.0246102.

- [66] R. L. Truby, C. D. Santina, and D. Rus. Distributed proprioception of 3d configuration in soft, sensorized robots via deep learning. *IEEE Robotics and Automation Letters*, 5:3299–3306, 2020. doi: 10.1109/lra.2020.2976320.
- [67] H. Yang and P. Hong-xia. The adaptive analysis of shock signals on the basis of improved morlet wavelet clusters. *Shock and Vibration*, 2018, 2018. doi: 10.1155/2018/9892713.
- [68] H. Li. Bearing fault diagnosis based on time scale spectrum of continuous wavelet transform. *2011 Eighth International Conference on Fuzzy Systems and Knowledge Discovery (FSKD)*, 2011. doi: 10.1109/fskd.2011.6019822.
- [69] H. Yi and S. Y. Hong. The improvement of the morlet wavelet for multi-period analysis of climate data. *Comptes Rendus. Géoscience*, 344:483–497, 2012. doi: 10.1016/j.crte.2012.09.007.
- [70] Q. Pang, L. Kuang, Y. Xu, and X. Dai. Study on the extraction and reconstruction of arbitrary frequency topography from precision machined surfaces. *Proceedings of the Institution of Mechanical Engineers, Part B: Journal of Engineering Manufacture*, 233:1772–1780, 2018. doi: 10.1177/0954405418802307.
- [71] Jonathan M Lilly and Sofia C Olhede. Generalized morse wavelets as a superfamily of analytic wavelets. *IEEE Transactions on Signal Processing*, 60(11):6036–6041, 2012.
- [72] Sanjit K Mitra. *Digital signal processing: a computer-based approach*. McGraw-Hill Higher Education, 2001.
- [73] Ahmed Silik, Mohammad Noori, Wael A Altabey, Ramin Ghiasi, and Zhishen Wu. Comparative analysis of wavelet transform for time-frequency analysis and transient localization in structural health monitoring. *Structural Durability and Health Monitoring*, 15(1):1, 2021.
- [74] Jonathan M Lilly and Sofia C Olhede. Higher-order properties of analytic wavelets. *IEEE Transactions on Signal Processing*, 57(1):146–160, 2008.
- [75] Ingrid Daubechies, Jianfeng Lu, and Hau-Tieng Wu. Synchrosqueezed wavelet transforms:

- An empirical mode decomposition-like tool. *Applied and computational harmonic analysis*, 30(2):243–261, 2011.
- [76] Gaurav Thakur, Eugene Brevdo, Neven S Fučkar, and Hau-Tieng Wu. The synchrosqueezing algorithm for time-varying spectral analysis: Robustness properties and new paleoclimate applications. *Signal Processing*, 93(5):1079–1094, 2013.
- [77] Stéphane Mallat. *A wavelet tour of signal processing*. Academic Press, 2008.
- [78] Muhammad Rehan, Muhammad Mubasher Saleem, Mohsin Islam Tiwana, Rana Iqtidar Shakoor, and Rebecca Cheung. A soft multi-axis high force range magnetic tactile sensor for force feedback in robotic surgical systems. *Sensors*, 22(9):3500, 2022.
- [79] Huiwen Yang, Ling Weng, Bowen Wang, and Wenmei Huang. Design and characterization of high-sensitivity magnetostrictive tactile sensor array. *IEEE Sensors Journal*, 22(5):4004–4013, 2022.
- [80] Luca Massari, Giulia Fransvea, Jessica D’Abbraccio, Mariangela Filosa, Giuseppe Terruso, Andrea Aliperta, Giacomo D’Alesio, Martina Zaltieri, Emiliano Schena, Eduardo Palermo, et al. Functional mimicry of ruffini receptors with fibre bragg gratings and deep neural networks enables a bio-inspired large-area tactile-sensitive skin. *Nature Machine Intelligence*, 4(5):425–435, 2022.
- [81] R Atoche-Enseñat, E Pérez, A Hernández-Benítez, A Balam, Johan J Estrada-López, J Vázquez-Castillo, F Avilés, and A Castillo-Atoche. A smart tactile sensing system based on carbon nanotube/polypropylene composites for wearable applications. *IEEE Sensors Journal*, 2022.